TGFβ2 and TGFβ3 isoforms drive fibrotic disease pathogenesis

Authors:

Tianhe Sun[1,*], Zhiyu Huang[2], Wei-Ching Liang[3], Jianping Yin[4], Wei Yu Lin[3], Jia Wu[3], Jean-Michel Vernes[5], Jeff Lutman[6], Patrick Caplazi[7], Surinder Jeet[2], Tiffany Wong[4], Manda Wong[4], Daryle J. DePianto[1], Katrina B. Morshead[1], Kai-Hui Sun[8], Zora Modrusan[8], Jason A. Vander Heiden[9], Alexander R. Abbas[9], Hua Zhang[2], Min Xu[2], Elsa-Noah N'Diaye[1], Meron Roose-Girma[10], Paul J. Wolters[11], Rajbharan Yadav[6], Siddharth Sukumaran[6], Nico Ghilardi[1], Racquel Corpuz[4], Claire Emson[2], Y. Gloria Meng[5], Thirumalai R. Ramalingam[12], Patrick Lupardus[4], Hans D. Brightbill[2], Dhaya Seshasayee[3], Yan Wu[3] and Joseph R. Arron[1,*]

Affiliations:

[1]Department of Immunology Discovery, Genentech, 1 DNA Way, South San Francisco, CA 94080, USA.

[2]Department of Translational Immunology, Genentech, 1 DNA Way, South San Francisco, CA 94080, USA.

[3]Department of Antibody Engineering, Genentech, 1 DNA Way, South San Francisco, CA 94080, USA.

[4]Department of Structural Biology, Genentech, Inc., 1 DNA Way, South San Francisco, CA 94080, USA.

[5]Department of Biochemical and Cellular Pharmacology, Genentech, 1 DNA Way, South San Francisco, CA 94080, USA.

[6]Department of Preclinical and Translational Pharmacokinetics, Genentech, 1 DNA Way, South San Francisco, CA 94080, USA.

[7]Department of Pathology, Genentech, Inc., 1 DNA Way, South San Francisco, CA 94080, USA.

[8]Department of Protein Sciences, Genentech, Inc., 1 DNA Way, South San Francisco, CA 94080, USA.

[9]Department of OMNI Bioinformatics, Genentech, Inc., 1 DNA Way, South San Francisco, CA 94080, USA.

[10]Department of Molecular Biology, Genentech, Inc., 1 DNA Way, South San Francisco, CA 94080, USA.

[11]Department of Medicine, University of California, San Francisco, CA 94143, USA.

[12]Department of Biomarker Discovery OMNI, Genentech, Inc., 1 DNA Way, South San Francisco, CA 94080, USA.

*Correspondence: sun.tianhe@gene.com (T.S); arron.joseph@gene.com (J.R.A.).

ABSTRACT

Transforming Growth Factor-beta (TGFβ) is a key driver of fibrogenesis. Three TGFβ isoforms (TGFβ1, 2 and 3) in mammals have distinct functions in embryonic development; however, the postnatal pathological roles and activation mechanisms of TGFβ2 and TGFβ3 have not been well characterized. Here we show that the latent forms of TGFβ2 and TGFβ3 can be activated by integrin-independent mechanisms and have lower activation thresholds compared to TGFβ1. Unlike *TGFB1, TGFB2* and *TGFB3* expression is increased in human lung and liver fibrotic tissues compared to healthy control tissues. Thus, TGFβ2 and TGFβ3 may play a pathological role in fibrosis. Inducible conditional knockout mice and anti-TGFβ isoform selective antibodies demonstrated that TGFβ2 and TGFβ3 are independently involved in mouse fibrosis models in vivo, and selective TGFβ2 and TGFβ3 inhibition does not lead to the increased inflammation observed with pan-TGFβ isoform inhibition. A co-crystal structure of a TGFβ2-anti-TGFβ2/3 antibody complex reveals an allosteric isoform-selective inhibitory mechanism. Therefore, inhibiting TGFβ2 and/or TGFβ3 while sparing TGFβ1 may alleviate fibrosis without toxicity concerns associated with pan-TGFβ blockade.

One Sentence Summary:

TGFβ2 and TGFβ3 isoforms are activated via unique mechanisms and are associated with fibrosis in human diseases.

INTRODUCTION

In mammals, TGFβ comprises a pleiotropic set of three cytokines - TGFβ1, TGFβ2, and TGFβ3 – that play critical roles in cell differentiation, tissue development, wound repair, immunomodulation, and, when dysregulated, tissue fibrosis. In the case of interstitial lung diseases (ILD) such as idiopathic pulmonary fibrosis (IPF), TGFβ activity is involved in multiple aspects of disease pathogenesis, including promoting apoptosis of lung epithelial cells and activation, differentiation, and survival of myofibroblasts and their production of extracellular matrix (ECM) (*1*). Aberrant TGFβ signaling is associated with other chronic fibrotic disorders including non-alcoholic steatoheptatitis (NASH), and systemic sclerosis (SSc)/scleroderma (*2, 3*). Although these findings implicate TGFβ as a potential therapeutic target for fibrotic disorders, the specific postnatal contributions of individual TGFβ isoforms have not been well studied.

TGFβ1, 2, and 3 are encoded by separate genes that are highly conserved across vertebrates. Full length pro-TGFβ is translated as a single peptide that is subsequently cleaved by furin proteases in the Golgi. Heterotetramers of the two resulting peptides form non-covalent interactions between the latency-associated peptide (LAP) and receptor-binding domain (interchangeably referred to as “mature peptide”, “growth factor,” or “cytokine” domain), termed the small latent complex (SLC) or “latent” TGFβ, in which a dimer of the receptor-binding domain is “caged” within a dimer of the LAP. Latent TGFβ1 does not induce intracellular signals unless it is activated to release the receptor-binding domain either by protease-mediated LAP cleavage or by mechanical forces between “milieu” molecules and cell surface integrins via binding of an arginine-glycine-aspartate (RGD) motif in the LAP (*3-5*). These activation mechanisms have been extensively studied in the case of TGFβ1, but it is not clear whether TGFβ2 and TGFβ3 are activated via similar mechanisms. Although all three isoforms are processed similarly to produce a SLC, there may be differences in how receptor-binding domains are

released. For example, whereas TGFβ3 has an RGD motif in its LAP domain and under certain conditions shows evidence of integrin-dependent activation, TGFβ2 lacks an RGD motif and is thus likely not activated via conventional integrin binding.

Genetic deletion studies have revealed distinct roles for the three TGFβ isoforms in development and homeostasis. TGFβ1 knockout mice survive to birth, but develop a spontaneous lethal autoinflammatory syndrome and die by 3-4 weeks of age (*6, 7*); TGFβ2 and TGFβ3 knockout mice die perinatally with cleft palates and inability to suckle. TGFβ2 knockout mice also exhibit multiple cardiovascular developmental anomalies (*8*). TGFβ3 knockouts are reported to have normal cardiovascular development but exhibit modest developmental delays in lung morphogenesis (*9, 10*). Although the autoinflammatory phenotype of TGFβ1 deficiency is recapitulated in adult animals in bone marrow chimeras (*11*), the postnatal roles of TGFβ2 and TGFβ3 have not been well characterized.

Although some of these phenotypes including cleft palate may be due to a requirement for TGFβ activity during specific embryonic developmental windows, others including autoinflammation present more of a concern with pharmacologic TGFβ inhibition postnatally. Several inhibitors of TGFβ signaling have been investigated in preclinical toxicology studies, including small molecule inhibitors of the kinase activity of TGFβR1 (ALK5) (*12, 13*) and pan-TGFβ antibodies that can inhibit all three isoforms (*14*). These agents have been associated with bleeding and cardiotoxicity which limits their potential for clinical development in chronic diseases. Therefore, although TGFβ is a central player in pathological fibrosis and remains a compelling therapeutic target, its roles in tissue homeostasis and immunoregulation present major challenges in establishing a suitable therapeutic index for its inhibition. A greater understanding of TGFβ isoform expression patterns and molecular activation mechanisms may reveal opportunities to

modulate TGFβ signaling with sufficient efficacy and safety to offer therapeutic benefit to patients with fibrotic disorders. To address this possibility, we investigated activation mechanisms and expression patterns of the three TGFβ isoforms in contexts relevant to human fibrotic disorders, developed highly potent and isoform selective inhibitory monoclonal antibodies against TGFβ2 and β3, and assessed their activity in preclinical models.

RESULTS

Full length TGFβ3 conditioned media inhibits alveolosphere formation in vitro

The lung alveolar epithelium is maintained and repaired by proliferation and hyperplasia of type 2 alveolar epithelial cells (AEC2), followed by differentiation into type 1 alveolar epithelial cells (AEC1). To investigate AEC biology, we employed a 3-D alveolosphere organoid culture system, in which fate-mapped AEC2s were isolated from *Sftpc-CreER^{T2};Rosa26R-tdTm* mice after tamoxifen induction and co-cultured with lung fibroblasts in Matrigel. After ~14 days, spheroids derived from individual AEC2s have developed, with an outer layer of AEC2s and an inner lumen with AEC1s that have differentiated from AEC2 progenitors (*15*). We have previously employed this system to identify TAZ as a regulator of AEC2-AEC1 differentiation during alveolar repair (*16*). To identify factors that affect alveolar epithelial cell proliferation, we screened an expression plasmid library carrying approximately 1,700 individual human genes encoding secreted proteins. We transiently transfected this plasmid library into 293T cells, first in pools (10-20 individual plasmids/pool) and subsequently individually, harvested the conditioned media two days later, and added conditioned media to alveolosphere cultures (schematic, Fig. 1A). There was no alveolosphere formation in the conditioned media from cells transfected with a construct encoding full-length TGFβ3. In contrast, conditioned media from cells transfected with full-length TGFβ1 had no qualitative effect on alveolosphere formation, despite using the same transfection

conditions and expression vectors (Fig. 1, B-D). Prior studies have shown that the receptor-binding domain ("mature" form) of TGFβ1 can promote apoptosis of primary type 2 alveolar epithelial cells (AEC2) in vitro (*17*) and in vivo (*18*). Accordingly, we observed no alveolosphere formation upon treatment with the recombinant mature forms of TGFβ1 or TGFβ3 (Fig. 1, E-G; schematic structures of constructs in H). Therefore, under the culture conditions used, full length LAP-associated TGFβ1 is inactive, but full length LAP-associated TGFβ3 is active, suggesting that "latent" TGFβ3 has intrinsic activity and/or it can be activated by a unique mechanism presented in this culture system, distinct from those described for TGFβ1.

Full-length TGFβ2 and TGFβ3 can activate TGFβR-dependent signaling independent of integrin binding in vitro

As integrin binding is an established mechanism of TGFβ1 activation, and we observed differential activity of TGFβ1 and TGFβ3 in the alveolosphere model, we sought to determine the integrin dependence of TGFβ3 activation. We used a 2-cell in vitro reporter system, in which expression vectors encoding full-length TGFβ1 or TGFβ3 were co-transfected into 293T cells with expression vectors encoding αv and β6 integrins, and co-cultured with a reporter cell line driving luciferase expression downstream of a SMAD-dependent promoter element ("MLEC", (*19*)) (Schematic, Fig. 2A). We found that whereas full-length TGFβ1 required co-expression of αvβ6 integrin to induce reporter activity, full-length TGFβ3 robustly induced reporter activity without co-transfection of αv and β6 integrin constructs. Co-expression of αvβ6 further increased full-length TGFβ3 dependent reporter activity by 51%, and this further increase was attenuated by mutation of the RGD integrin-binding motif in the LAP of TGFβ3 to RGE (Fig. 2B). Consistent with the observed effects from the alveolosphere experiment described above, supernatants from cells transfected with full-length TGFβ3, but not TGFβ1, robustly induced reporter activity (Fig. 2C). We observed similar reporter

induction with supernatants from full-length TGFβ2-transfected cells; as TGFβ2 lacks an RGD motif (Fig. S1), its activation is likely integrin-independent (Fig. 2C). Total TGFβ activities from these three supernatants were comparable after an acidification step, which releases the receptor-binding domain of TGFβ from its latent complex (*20, 21*) (Fig. 2C). To rule out the possibility that these effects were specific to the reporter cell lines we used, we assessed HEK-Blue (InvivoGen) and SCOS-7 cells as alternative TGFβ reporter and transfection recipient cell lines, respectively, and observed high "intrinsic" activities of TGFβ2 and/or TGFβ3 in both cases (Fig. S2, A and B). Cytoskeletal tension is required to transduce forces during integrin αvβ6-mediated activation of latent TGFβ1 (*22*). To discount the possible involvement of other cytoskeleton-dependent integrin activities, we treated this culture system with cytochalasin D to inhibit actin polymerization, which attenuated the integrin αvβ6-mediated activation of TGFβ1 and TGFβ3. However, the "intrinsic" activity of TGFβ3 remained unaffected (Fig. S2C), suggesting that this activity is αvβ6 integrin independent.

In the Golgi apparatus, the pro-peptide of TGFβ1 (pro-TGFβ1) is proteolytically cleaved by furin, leading to SLC formation (Fig. 1H) (*23*). This proteolytic digestion is essential to generate functional TGFβ1. All three TGFβ isoforms have conserved furin cleavage sites (RKKR or RHRR, Fig. S1). To assess the requirement for this protease cleavage for TGFβ2/3 activity in our system, we mutated the furin cleavage sites in each TGFβ isoform (Fig. S2D). Mutated full-length TGFβ2 and β3 completely lost their intrinsic activities (Fig. S2E). Thus, like TGFβ1, furin cleavage is required for TGFβ2/3 activity, despite distinct extracellular activation mechanisms of the SLCs. To evaluate the kinetics of “intrinsic” TGFβ2 and TGFβ3 activity, we assessed phospho-SMAD2 in normal human lung fibroblasts (NHLF) after treatment with transfection supernatants and

observed similar kinetics to cells treated with recombinant TGFβ receptor-binding domains, with pSMAD2 peaking about 1 h after stimulation (Fig. S2F).

To discount the possibility that other factors present in the conditioned media of transfected cells could contribute to TGFβ2 and TGFβ3 activation, we generated recombinant full-length TGFβ isoforms. To improve expression and stability and facilitate purification, we made in-frame N-terminal fusions of the constant domain of human IgG1 ("Fc") to each isoform (Fc-FL-TGFβ1, 2, and 3). Consistent with the effects we observed in conditioned media, purified recombinant Fc-FL-TGFβ1 did not activate reporter activity in MLEC. However, Fc-FL-TGFβ2 and Fc-FL-TGFβ3 robustly induced reporter activities (Fig. 2D), which were inhibited by their respective isoform-specific antibodies (Fig. 2E).

Previous studies showed that recombinant LAP from TGFβ1 (LAP1) can strongly inhibit the receptor-binding domains of TGFβ1, 2, and 3 in vitro and in vivo, presumably by reconstituting them into SLCs (*24*). Whereas the receptor-binding domains of TGFβ isoforms are highly homologous, the LAP domains are more diverse (Fig. S2G). Thus, we postulated that the LAPs from TGFβ1, 2, and 3 (LAP1, 2 and 3, respectively) might have differential inhibitory capacities. We generated recombinant N-terminal fusion proteins of human IgG1 with human LAP1, 2, and 3 (Fc-LAP1, 2, and 3), and observed substantially different neutralization capabilities for each Fc-LAP. Consistent with our observations with conditioned media and recombinant full-length TGFβ proteins, Fc-LAP1 more potently inhibited the receptor-binding domains of all three TGFβ isoforms than Fc-LAP2 or Fc-LAP3 (Fig. 2, F-I). Taken together, these data show that the relative potencies of LAP1, 2, and 3 to inhibit TGFβ activity are divergent and suggest that the "intrinsic" activities of full-length TGFβ2 and TGFβ3 not observed for TGFβ1 are conferred by the respective LAP domains of these isoforms.

In addition, the findings support the idea that FL-TGFβ2 and TGFβ3 may have distinct activation mechanisms and thresholds from those of TGFβ1. Although FL-TGFβ1 can be activated by ectopic expression of αvβ6 integrin, and FL-TGFβ3's activity can be increased by αvβ6 integrin binding, both FL-TGFβ2 and FL-TGFβ3 appear to have "intrinsic" activities, and/or are activated by as-yet unidentified mechanisms. The biochemical inhibitory potencies of LAP1, 2, and 3 are divergent, with the biochemical IC50 of LAP1 against each receptor-binding isoform being several orders of magnitude lower than those of LAP2 and LAP3. Given that latent TGFβ1 has a much higher threshold for activation than latent TGFβ2 or TGFβ3, our mechanistic observations suggest that TGFβ2 and TGFβ3 gene expression are more likely than TGFβ1 gene expression to reflect their activities in tissue.

TGFβ2 and TGFβ3 expression is elevated and TGFβ3 expression localizes to fibroblastic foci in human IPF tissue

As a key driver of tissue fibrosis, TGFβ activity is locally restricted in an autocrine or paracrine fashion (*5*). Given our observations that TGFβ2 and TGFβ3 may be active in their "latent" forms and/or are more readily activated than TGFβ1, we evaluated the expression patterns of TGFβ isoforms in tissues from human fibrotic disorders. In gene expression microarray analyses of bulk lung biopsy samples (*25*), *TGFB3*, and to a lesser extent, *TGFB2,* had significantly higher expression in IPF compared to control lungs ($P < 0.0001$ and $P < 0.01$, respectively), whereas *TGFB1* expression was similar in IPF and control (Fig. 3A). Immunohistochemistry revealed abundant increases in nuclear phospho-SMAD2/3 staining in IPF tissue as compared to control, as illustrated in fibroblastic foci, which are regions of activated fibroblasts and myofibroblasts pathognomonic for a histological diagnosis of Usual Interstitial Pneumonia (UIP), the hallmark of IPF (Fig. 3B). As differences in gene expression in bulk IPF lung tissue may

reflect cytological composition of the sample (*25*), we sought to characterize the cellular provenance of TGFβ isoforms on a single-cell basis using single-cell RNA sequencing (scRNAseq). Global gene expression patterns of scRNAseq data from IPF lungs distinguished multiple cell lineages including hematopoietic (macrophages, lymphocytes, mast cells), epithelial (basal, ciliated, and secretory bronchial epithelial cells and AEC2), mesenchymal (fibroblasts, myofibroblasts, smooth muscle), and vascular (endothelial) cell types (Fig. 3C, S3A and S3B). *TGFB1* was broadly expressed, with highest expression in hematopoietic cells, endothelial cells, and myofibroblasts. *TGFB2* was more restricted and primarily detected in epithelial cells. *TGFB3* expression was most highly expressed in mesenchymal cells (fibroblasts, myofibroblasts, and smooth muscle cells). Expression of TGFβR-dependent target genes revealed distinct patterns, with *SERPINE1* expressed in fibroblasts, macrophages, and endothelial cells, and *COL1A1* in myofibroblasts; the latter largely overlapping with *TGFB3* (Fig. 3D). Dual immunohistochemistry for pSMAD3 and in situ hybridization for *TGFB3* revealed numerous myofibroblasts in fibroblastic foci co-expressing *TGFB3* and nuclear pSMAD3, suggesting that in UIP lesions, TGFβ3 may be driving TGFβR-dependent signaling to promote collagen expression in an autocrine or paracrine fashion (Fig. 3E and Fig. S3C).

TGFβ2 and TGFβ3 conditional KO mice have decreased lung fibrosis in a bleomycin challenge model

Intratracheal (i.t.) bleomycin challenge is a frequently used in vivo rodent model of lung fibrosis. Bleomycin selectively injures alveolar epithelial cells, triggering an innate immune response followed by fibroblast differentiation into myofibroblasts and ECM deposition. Unlike a chronic, progressive condition such as IPF, the bleomycin model has specific phases: injury, inflammation, fibrosis, and, in young animals, resolution (*26*). To assess the kinetics of TGFβ isoform expression in this model, we assessed lung gene

expression in mice at various timepoints after i.t. bleomycin instillation in a published transcriptomic dataset (*27*). Whereas *Tgfb1* expression was not elevated in bleomycin-challenged mice at any timepoint and decreased at days 21 and 28, *Tgfb2* and *Tgfb3* expression were substantially increased after bleomycin installation at day 7 and day 14 after challenge (Fig. 4A). This pattern overlapped well with the induction of genes associated with fibrogenesis and TGFβ signaling, such as *Serpine1, Fn1,* and *Col1a1* (Fig. 4B). The upregulation of *Tgfb2* and *Tgfb3* during the fibrotic phase of the model concurred with expression pattern observed in IPF lung (Fig. 3A). To further characterize the specific cell types responsible for the expression of each TGFβ isoform in this model, we performed RNAseq on sorted lung cell populations day 14 after bleomycin administration when multiple fibrosis-associated genes peaked (Fig. S4). Consistent with scRNAseq data from human IPF lung tissue (Fig. 3D), leukocytes ($CD45^+$) had the highest *Tgfb1* expression. *Tgfb2* and *Tgfb3* were predominantly expressed in fibroblasts ($CD45^-$, $EpCAM^-$ $CD31^-$); *Tgfb2* was also induced in epithelial cells and TGFβR-inducible genes *Col1a1* and *Serpine1* were induced mainly in fibroblasts after bleomycin treatment. Although we did not observe substantial upregulation of *Tgfb3* in any individual cell populations after bleomycin treatment, we attribute the substantial upregulation in *Tgfb3* in bulk lung tissue (Fig. 4A) to increased proportions of *Tgfb3*-expressing fibroblasts at those timepoints.

As constitutive deletion of *Tgfb2* or *Tgfb3* results in embryonic or perinatal lethality (*8-10*), we generated inducible knockouts of these genes to investigate their roles in bleomycin-induced lung fibrosis in adult animals, by introducing loxP sites in *Tgfb2 (*$Tgfb2^{fl/fl}$*)* and *Tgfb3 (*$Tgfb3^{fl/fl}$*),* respectively (Fig. S5). We crossed $Tgfb2^{fl/fl}$, $Tgfb3^{fl/fl}$, and $Tgfb2^{fl/fl}/Tgfb3^{fl/fl}$ to *ROSA-*$CreER^{T2}$, and dosed 12-16 week old mice with tamoxifen to delete the respective TGFβ alleles (single conditional KO mice will be referred to as TGFβ2.cKO and TGFβ3.cKO, and double targeted mice will be referred to as

TGFβ2/3.cDKO). No gross abnormalities or morbidities were observed in cKO animals up to 6 weeks after tamoxifen treatment. To assess the roles of TGFβ2 and TGFβ3 in lung fibrosis, we treated adult cKO animals with tamoxifen starting 2 weeks before bleomycin administration. From days 9-24 after bleomycin administration, we administered deuterated drinking water to assess new collagen synthesis in whole lungs by measuring deuterated hydroxyproline (Fig. 4C) (*16*). In both TGFβ2.cKO and TGFβ3.cKO mice, as well as in TGFβ2/3.cDKO mice, new collagen synthesis was significantly reduced ($P < 0.05$, $P < 0.05$ and $P < 0.001$, respectively), suggesting that both TGFβ2 and TGFβ3 contribute to fibrogenesis in this model (Fig. 4, D and E).

Generation of isoform-selective TGFβ2 and TGFβ3 antibodies

We generated monoclonal antibodies from rats and rabbits immunized with the mature receptor-binding domains of human TGFβ2 and TGFβ3 and screened them for binding via direct enzyme-linked immunosorbent assay (ELISA) and surface plasmon resonance (SPR), and for their ability to inhibit mature receptor-binding domain induced TGFβR-dependent signaling in reporter cell lines. We identified potent inhibitory antibodies (K_D < 10 pM and cell-based IC50 <250 pM) with selectivity for TGFβ2 (6F12), TGFβ3 (2A10), and a dual-specificity antibody that bound to and inhibited the activity of both TGFβ2 and TGFβ3 (4A11) (Table S1). None of these substantially bound to, nor functionally inhibited, TGFβ1. The relative potencies of these antibodies for selected TGFβ isoforms were comparable or superior to the activity of a pan-TGFβ antibody, 1D11 (Table S1). The TGFβ2-specific antibody 6F12 was nearly 100-fold more potent than 1D11 in blocking TGFβ2-dependent reporter activity in cells (IC50 of 40 pM vs. 3.6 nM). There are three amino acid differences between human and mouse mature TGFβ2, and 6F12 and 4A11 bind to both peptides with similar affinities (Fig. S6A) and have similar inhibitory potencies against both (Fig. S6B). Mature TGFβ3 peptides are 100% homologous between human and mouse. We fused the Fab regions of these antibodies to

the Fc region of mouse IgG2a with a LALA-PG mutation to eliminate effector function for in vivo mouse studies (*28*). Whereas TGFβ1 and TGFβ3 strongly bind to TGFβR2, TGFβ2 binds weakly to both TGFβR1 and TGFβR2 (*29*). TGFβR3 (betaglycan) can enhance TGFβ2 binding to the TGFβR1-TGFβR2 receptor complex (*30*). We sought to determine whether these antibodies can block the binding of the ligands to TGFβR chains (Table S1). Both 1D11 and 2A10 inhibited binding of TGFβR2 to TGFβ ligands (Fig. S7), suggesting that they share similar binding epitopes with this receptor. Although 2A10 can inhibit binding of both TGFβ2 and TGFβ3 to TGFβR2 under these assay conditions with high concentrations of binding partners, it does not block TGFβ2-induced signals at the lower concentrations employed in in vitro and in vivo studies shown in subsequent experiments. Fresolimumab has been shown to bind to a similar epitope on TGFβ isoforms that interacts with TGFβR1/2 (*31, 32*). In contrast, 6F12 altered the kinetics of TGFβ2 binding to TGFβR2 by modestly reducing its on/off rates (Fig. S7), and strongly inhibited TGFβR3 binding to TGFβ2 (Table S1), suggesting a different, TGFβ2-specific mode of inhibition. In contrast to the other antibodies, 4A11 enhanced SPR signals in the presence of TGFβR2 and TGFβ2/3 (Fig. S7), suggesting that 4A11 binds to an epitope that does not directly interfere with TGFβ2/3-TGFβR2 interactions.

Structural analysis of the anti-TGFβ2/3 dual specific antibody 4A11 reveals an allosteric inhibitory mechanism

As 4A11 does not directly interfere with TGFβ2/3 binding to TGFβR2, we performed structural studies to determine its inhibitory mechanism and isoform selectivity. The rabbit 4A11 antibody was first humanized to enable non-human primate pharmacokinetics and safety studies, as well as future human clinical trials. Humanized 4A11 was generated on a human IgG1.N297A (effector attenuated) backbone, had comparable functional characteristics to the parental rabbit 4A11 antibody and was selected for crystallography (Table S2).

A crystal complex structure of 4A11 bound to the mature form of human TGFβ2 at 1.91Å with R/Rfree statistics of 20.5/24.4% was solved (Table S3). The epitope for 4A11 is on the underside of the TGFβ2 dimer, with the two Fabs bound to two identical epitopes as expected for a symmetric homodimer (Fig. 5A). The epitope for each arm of 4A11 encompasses TGFβ2 residues V313, Q314, D315, R320, L322, Y323, R328, D329, F345, and A347 in one TGFβ2 monomer, and N368, T369, I370, N371, P372, E373, A374, S375, A376, and S377 in the second TGFβ2 monomer (Fig. 5B and Table S4), with ~1950 $Å^2$ of surface area buried. The 4A11 epitope is centered on the cap of an alpha helix (residue 359-372). Within the epitope, there is considerable sequence conservation between TGFβ1, 2, and 3, but one major difference observed in TGFβ1 but not TGFβ2/3 is a change from glutamate to glycine at position 373 (human TGFβ2 numbering) (Fig. 5C and Table S5). This glutamate residue lies at the center of the 4A11 epitope, and the carboxylic acid side chain makes a polar contact with CDR H1 T33 (Fig. 5C). A change from glutamate to glycine would disrupt this side chain-mediated polar interaction and remove a large amount of buried surface area.

Dimeric TGFβ ligands bind to the TGFβR1/R2 complex via their "fingertip" regions (Fig. S8A) (*29, 33*). Unlike previously described anti-TGFβ blocking antibodies such as fresolimumab (Fig. S8B) (*31, 32*), the 4A11 epitope is not near the TGFβR1/TGFβR2 binding sites, and neither 4A11 Fab sterically competes for receptor binding. Instead, the 4A11 Fabs appear to induce a conformational change in TGFβ2, causing the two monomers to "pinch" together by several degrees (Fig. 5, D and E). Comparison of the 4A11 bound TGFβ2 and a previously described structure of TGFβ3 bound to TGFβR1 and TGFβR2 (*33*) suggests that the receptor binding site for at least one of the TGFβ2 monomers is compromised by this conformational change (Fig. 5F). This indicates that 4A11 inhibits TGFβ2/3 via an allosteric mechanism by conformational disruption of one

of the receptor binding sites. Hence, bivalent binding of a 4A11 IgG molecule would be required to induce this conformational change in TGFβ2/3 to thereby inhibit TGFβ2/3 signaling. Our SPR results further suggested that one of the receptor binding sites of TGFβ2/3 may still be functional in the presence of 4A11 (Table S1, Fig. S7). Moreover, given the location of the epitopes, divalent binding of a full 4A11 IgG molecule may also sterically prevent an IgG bound TGFβ2/3 molecule from getting close enough to the membrane to access TGFβ receptors. Taken together, these structural observations demonstrate an allosteric mechanism of TGFβ2/3 inhibition by the 4A11 antibody that does not rely on steric interference with the receptor, but instead requires divalent binding to the TGFβ dimer to prevent signaling.

Pharmacokinetics of anti-TGFβ isoform-specific antibodies in C57BL/6 mice

Pharmacokinetics (PK) of three chimeric antibodies (6F2, 2A10, and 4A11) were characterized following a single intravenous (IV) dose of 1 or 10 mg/kg, or intraperitoneal (IP) dose of 10 mg/kg in female C57BL/6 mice. All three antibodies demonstrated favorable PK profiles, with apparent biphasic distribution characterized by a short distribution phase followed by a longer elimination phase. Linear and dose-proportional (C_{max} and AUC; area under the concentration-time curve) PK were observed between 1 and 10 mg/kg, with clearance ranging from 3.5 to 4.9 mL/day/kg in all cohorts (Table S6). Following single IP administration of 6F2 and 4A11 at 10 mg/kg, the AUC_{last} was ≥97% and C_{max} was ~50-60% when comparing the AUC_{last} and C_{max} after IV administration at 10 mg/kg (Table S6).

In vivo activity of isoform-selective anti-TGFβ2 and TGFβ3 antibodies in a lung fibrosis model

To assess the in vivo effects of anti-TGFβ2 (6F12) anti-TGFβ3(2A10), and dual-TGFβ2/TGFβ3 inhibitory (4A11) antibodies on lung fibrosis, we treated mice

preventively and examined TGFβ induced gene expression in lungs at day 14 after bleomycin administration, when the expression of those genes peaked (schematic, Fig. 4C). *Serpine1, Fn1,* and *Col1a1* expression were all substantially reduced in mice treated with either single isoform-selective antibody (Fig. 6, A and B). Dual TGFβ2 and TGFβ3 inhibition via 4A11 treatment reduced new collagen accumulation at day 24 comparably to the combination of both 6F12 and 2A10 (Fig. 6C). We performed a dose titration of 4A11 and observed comparable efficacy at doses of 10mg/kg thrice or once weekly, but not at 3 mg/kg/week (Fig. 6C). Pathologic examination of lungs at day 24 showed greatly attenuated disease scores and collagen accumulation in the high-dose 4A11 treated group compared to the control group (Fig. 6, D and E). Taken together, these data show that treatment with neutralizing antibodies to TGFβ2 and TGFβ3 can reduce lung fibrosis in vivo.

TGFβ2 and TGFβ3 contribute to hepatic fibrosis

To extend our observations beyond pulmonary fibrosis, we assessed TGFβ isoform gene expression in human NAFLD/NASH patient samples from a published dataset comparing mild to advanced fibrosis (GSE49541, (*34, 35*)). Similar to IPF lung tissue, *TGFB1* was comparable across disease severity, whereas both *TGFB2* and *TGFB3* were increased in livers from patients with more advanced fibrotic stages of disease (Fig. 7A). In the carbon tetracholoride (CCl_4)-induced liver injury and fibrosis model in mice (Fig. 7B), we observed upregulation of *Tgfb2* and *Tgfb3*, but not *Tgfb1* expression after 6 weeks of CCl_4 challenge (Fig. 7C). Anti-TGFβ2/3 antibody (4A11) treatment substantially attenuated collagen gene expression and histological disease scores in CCl_4-challenged mice (Fig. 7, D and E). Histological examination showed a reduction of fibrosis in the 4A11 treated group when compared to controls (Fig. 7F). Taken together, these data suggest that TGFβ2 and TGFβ3 inhibition can reduce hepatic fibrosis in vivo.

TGFβ2 and TGFβ3 blockade does not promote the enhanced immune responses associated with pan anti-TGFβ blockade

TGFβ signaling plays pivotal roles in the regulation of immune responses. Previous studies with genetic or pharmacological blockade of TGFβ signaling showed excessive inflammation and leukocyte infiltration in multiple organs, resulting in serious adverse toxicities (*12, 14, 36, 37*). To assess the contribution of TGFβ2 and TGFβ3 blockade to systemic immune responses, we employed the *Helicobacter hepaticus* infected IL-10R blockade colitis model (Fig. S9A). This model is often used to assess the involvement of dysregulated immune responses and intestinal microbiota, two major components of human inflammatory bowel diseases (IBD) (*38-40*). In agreement with previous findings (*40*), *H. hepaticus* infected mice treated with the anti-IL10R antibody developed colitis. Treatment with a pan-anti-TGFβ antibody (1D11) increased inflammation, as evidenced by increased colon weights, inflammatory cytokine expression, and immune cell infiltration (Fig. S9, B to D). However, mice treated with the TGFβ1-sparing anti-TGFβ2/3 antibody (4A11) exhibited no increases in inflammation on those parameters. These results suggest that selective TGFβ2/3 blockade will not induce toxic inflammatory responses as observed with pan-TGFβ blockade. Whether chronic selective inhibition of TGFβ2 and/or TGFβ3 contributes to other toxicities in the context of pathological fibrosis remains to be determined.

DISCUSSION

TGFβ is secreted from cells in a "latent" form in which its receptor-binding domain required for activity is shielded by a latency-associated peptide (LAP), which is in turn associated with a complex network of "milieu" molecules that restrict TGFβ activity to specific cellular contexts. There are three TGFβ isoforms with highly homologous receptor-binding domains that have similar effects on target cells in vitro, but with

divergent primary amino acid sequences in the LAP domains. However, the primary sequence of each respective LAP is highly conserved across species (*41*). This suggests that the biological functions of the three TGFβ isoforms are conserved across species but distinct and specialized among isoforms, and that differential activation mechanisms of the LAP domains, expression in different cell types, and different extracellular milieus are critical for conferring isoform-specific functions in vivo.

Previous studies have shown TGFβ isoforms to be expressed in different stages of fibrotic diseases (*42-45*). However, there was little evidence to show direct involvement of TGFβ2 and TGFβ3 in tissue fibrosis. In this study, we show that the "latent" forms of TGFβ2 and TGFβ3 have different mechanisms of and lower thresholds for activation than TGFβ1. These biochemical differences are important because gene expression patterns of *TGFB2* and *TGFB3* may be closely related to overall TGFβR signaling activity in complex tissues whereas TGFβ1 activity in complex tissues may depend more on its mechanisms of activation, through integrin binding, protease cleavage, or other mechanisms of LAP release. The lower activation thresholds and more restricted expression patterns for TGFβ2 and TGFβ3 may make active TGFβ available for tissue repair in response to acute injury, which can become maladaptive in a chronic setting, leading to fibrosis. In human patients with chronic fibrotic disorders with increased activity of TGFβR-dependent signaling such as IPF and NASH, *TGFB2* and *TGFB3* expression are elevated in lung and liver tissue, whereas *TGFB1* expression is not. *TGFB1* is broadly expressed, predominantly in hematopoietically derived cells in IPF lung, whereas *TGFB2* expression is more restricted to epithelial cells and *TGFB3* to mesenchymal cells. Genetic deletion or selective pharmacologic inhibition of TGFβ2 and/or TGFβ3 with potent and selective antibodies substantially reduces fibrosis in animal models of lung and liver fibrosis. Given the high homology between the receptor-binding domains of TGFβ isoforms, we have generated a unique antibody that recognizes

an epitope conserved in TGFβ2 and TGFβ3 but not in TGFβ1, and acts via an allosteric mechanism dependent on bivalent binding to TGFβ2 or TGFβ3. These findings support selective targeting of TGFβ2 and/or TGFβ3 to treat chronic fibrotic conditions while sparing the immunoregulatory functions of TGFβ1.

Integrin mediated TGFβ1 activation plays an important role during fibrosis (*22, 46, 47*). Using an in vitro reporter assay, we found that, whereas TGFβ1 did not exhibit integrin-independent intrinsic activity, TGFβ3 exhibited substantial intrinsic activity. However, this activity was increased by approximately 50% upon αvβ6 activation. Whereas the LAP domain of TGFβ1 potently inhibits the ability of mature TGFβ to bind to its receptors and activate signaling, the LAP domain of TGFβ3 is less inhibitory. Thus, unlike TGFβ1, TGFβ3 activity may be regulated in two ways: expression and integrin-augmented activation. Although we cannot determine the exact biological contexts for each activation mechanism, augmented integrin mediated TGFβ3 activity may enhance fibrosis in vivo, and the anti-fibrotic activity of integrin inhibitors may be due to both TGFβ1 and TGFβ3 inhibition. Although TGFβ1 plays roles in fibrosis (*48*), the contribution of different TGFβ isoforms to fibrosis is not mutually exclusive. Different TGFβ isoforms may execute their functions in spatially and temporally restricted manners. Indeed, we observed that the expression patterns of different isoforms are distinct in different cell lineages. Furthermore, the activity of one TGFβ isoform may regulate the expression or activation of other isoforms (*49*). Different TGFβ isoforms may also play their roles sequentially during the course of fibrosis. Ultimately, how TGFβ isoforms regulate each other in vivo is an interesting topic that requires further exploration, which may be facilitated by future clinical studies with isoform- and activation mechanism-selective interventions.

The receptor-binding domains of TGFβ1, 2, and 3 are highly homologous, with 83-90% amino acid similarity. Dimeric receptor-binding domains of all three isoforms bind to pairs of heterodimeric receptor complexes of TGFβR1 and TGFβR2; the tetrameric receptor complex then activates intracellular signaling via receptor serine/threonine kinase activity of TGFβR1 (ALK5). In canonical TGFβR signaling, ALK5 phosphorylates SMAD2 and SMAD3, which then associate with SMAD4, translocate to the nucleus, and direct gene transcription. Additional non-SMAD dependent signaling pathways such as MAP kinases, AKT, JAK-STAT, and NFκB may be activated downstream of TGFβRs in certain contexts (*5*). Biochemical and structural studies have shown that the assembly of TGFβ-TGFβR signaling complexes have subtle isoform-specific differences: TGFβ1 and TGFβ3 bind more strongly to TGFβR2 and only form strong interactions with TGFβR1 when in complex with TGFβR2, whereas TGFβ2 binds weakly to both TGFβR1 and TGFβR2 alone, and avidity may drive full complex formation (*29*). TGFβ1 and TGFβ2 crystallize in "closed" structures that facilitate binding to TGFβR1 and TGFβR2, whereas TGFβ3 can adopt a similar "closed" or less ordered "open" structure in crystal form, which may lead to differences in the avidity of ligand-receptor complex assembly (*50*). In addition, TGFβR3 (betaglycan), a non-signaling receptor, can specifically facilitate TGFβ2 binding to TGFβR1/2 complexes (*30*). Ultimately, despite these differences in signaling complex assembly, recombinant receptor-binding domains of TGFβ1, 2, and 3 are all able to induce TGFβR-dependent SMAD signaling to a similar degree in cell-based in vitro assays. Hence, any differences in the in vivo activity of endogenous TGFβ isoforms are more likely due to differences in their patterns of expression and mechanisms of release from SLC or LLC than to differences in their receptor-binding domains. Our SPR studies show that 2A10 blocks the TGFβR2 binding epitope of TGFβ3. 6F12, on the other hand, reduces the on/off binding rates of TGFβ2 and slows TGFβR2 binding kinetics, which may hamper TGFβR1 recruitment. Furthermore, 6F12 may inhibit TGFβ2 binding to the TGFβR

signaling complex by blocking TGFβR3. Future crystallography studies will be needed to better understand its inhibitory mechanism. Our structural analyses of the allosteric inhibitory mechanism of 4A11 suggest that bivalent antibody binding to a TGFβ2 or TGFβ3 dimer constrains TGFβ in a form that precludes simultaneous binding to two sets of receptor heterodimers. However, it is likely that TGFβR2 can still bind to one TGFβ monomer, as we observed enhanced signals in SPR in the presence of 4A11. These structural and epitopic studies illustrate multiple mechanisms of isoform-selective TGFβ inhibition.

The LAP domains of TGFβ1, 2, and 3 are substantially less homologous than the receptor-binding domains, with only 42-56% amino acid similarity (Fig. S1). All three isoforms have conserved furin cleavage sites (RKKR or RHRR) between the LAP and receptor-binding domains, and a conserved "fastener" sequence (YYAKE). TGFβ1 and TGFβ3 have an RGD integrin-binding sequence but TGFβ2 has an R-S substitution at that site and is not likely activated via integrin binding. Structures of the SLC including the LAP and receptor-binding domain have been solved for TGFβ1 but not for TGFβ2 or 3. The "finger" region of the receptor-binding domain of TGFβ1 that interacts with TGFβR2 is shielded by a "latency lasso", a loop between the α1 and α2 helices of the LAP that is associated with the fastener sequence. In all three isoforms, the C-terminal sequence of the LAP α1 helix is highly conserved, with a lysine residue (GQILS**K**L) that interacts with two conserved tyrosines (**YY**AKE) in the fastener of TGFβ1; in addition, the alanine (YY**A**KE) interacts with an arginine in the α5 helix near the C-terminus of the LAP that is conserved across the three isoforms (*51*). The latency lassos of the three TGFβ LAP isoforms exhibit some sequence diversity, with 6 prolines in TGFβ1, 5 in TGFβ2, and 4 in TGFβ3, and the length of the lasso is 1 and 2 residues shorter in TGFβ2 and TGFβ3, respectively, than in TGFβ1. There are substantial sequence differences between the three isoforms around the RGD integrin binding site: TGFβ2 has an SGD

sequence, does not likely bind integrins, and is 9 residues longer than TGFβ1 between the β9 and β10 strands; TGFβ3 has an RGD and is 3 residues longer than TGFβ1 between the β9 and β10 strands; and the loops between the β4 and β5 strands and β7 and β8 strands are substantially longer in TGFβ2 and TGFβ3 than they are in TGFβ1 (Fig. S1). Although structure-function relationships have not yet been elucidated for these regions, it is possible that they may contribute to different modes of activation and/or inhibitory potency of the LAP domains of TGFβ2 and TGFβ3 as compared to TGFβ1. Heterozygous loss-of-function mutations have been described in *TGFB2* and *TGFB3* genes associated with Loeys-Dietz syndrome (*52-54*) in key residues in the LAP domains, implicating the furin cleavage site in both, the fastener in TGFβ2, and the RGD integrin-binding site in TGFβ3, suggesting that these conserved motifs are important for at least some functions of TGFβ2 and TGFβ3. Whereas we show that full-length TGFβ2 and TGFβ3 carry "intrinsic" activity (Fig.s 1, 2 and S2), this activity remains dependent on furin cleavage (Fig. S2E), and in the case of TGFβ3, can be augmented by integrin binding (Fig. 2B and S2C). Consistent with the notion that the LAP, rather than the receptor-binding domain, confers activation specificity, we show that the LAP of TGFβ1 can potently inhibit all three isoforms, whereas the LAPs of TGFβ2 and TGFβ3 are much less inhibitory (Fig. 2, F-I).

Genetic deletion or inactivation of TGFβ1 or TGFβR2 in hematopoietic cells revealed a dominant immunoregulatory role, with progression of a lethal autoinflammatory syndrome over the first 4 weeks of life (*6, 7, 55*). Further studies established that the phenotype is transplantable in adult animals (*11*) and narrowed these effects primarily to CD4+ T cells and antigen-presenting cells (*36, 37, 56-59*). TGFβ1 also plays an important role in alveolar macrophage homeostasis, as conditional TGFβ1 deletion with an ITGAX-Cre transgenic results in progressive pulmonary alveolar proteinosis (*60*). On the other hand, TGFβ2 and TGFβ3 knockout mice die perinatally with cleft palates and

inability to suckle (*8-10*). Although deletion of either isoform yields cleft palates, the phenotypes are different: TGFβ2 knockouts have failure of palatal shelf rotation and no fusion of either the primary or secondary palate, whereas TGFβ3 knockouts have intact palatal shelf rotation but defective midline fusion. Thus, despite the biochemical similarities in the ability of the receptor-binding domains of the three TGFβ isoforms to induce signaling through TGFβR1 and TGFβR2, their expression patterns and activation mechanisms confer unique functions in embryonic development and homeostasis, particularly the dominant effect of TGFβ1 in immune regulation.

There are several rare human genetic disorders with heritable dominant loss-of-function mutations that affect TGFβ signaling, such as Marfan Syndrome, Shprintzen-Goldberg Syndrome, and Loeys-Dietz Syndrome (LDS) (*61*). Of these, LDS has been associated specifically with heterozygous loss-of-function mutations in *TGFBR1, TGFBR2, SMAD2, SMAD3, TGFB2,* and *TGFB3* that lead to decreased but not abolished TGFβ signaling. Although these mutations are compatible with life, LDS presents with multiple developmental morphogenic connective tissue abnormalities (*54, 62*). Loss-of-function mutations in *TGFB1* have generally not been observed in humans, although Camurati-Engelmann disease results from mutations in the LAP domain of *TGFB1* that attenuate the inhibitory activity of LAP, resulting in excessive TGFβ1 signaling in bone leading to cortical thickening and dysplasia (*63*).

Toxicology studies of ALK5 inhibitors (*12, 13*) or pan-TGFβ inhibitory antibodies (*14*) described extensive morbidities, including cardiac valvulopathies and bleeding. In humans, treatment with fresolimumab, a pan-TGFβ inhibitory antibody, resulted in bleeding, anemia, and an increased rate of keratoacanthomas that reversed with treatment cessation (*64, 65*). These observations suggest that bleeding, cardiac lesions, and epithelial hyperplasia are major concerns with long-term chronic pharmacologic pan-

TGFβ inhibition. However, our adult conditional knockout mice for TGFβ2 and/or TGFβ3 did not display any gross abnormalities or obvious morbidities up to 6 weeks after tamoxifen induction, nor did they exhibit any of the morbidities reported for pan-TGFβ inhibitors, and they were protected from fibrosis upon bleomycin treatment. Furthermore, unlike pan anti-TGFβ inhibition, selective TGFβ2/3 blockade was not associated with the increased inflammation in a colitis model. Longer-term assessments of these animals and those treated with isoform-selective TGFβ inhibitors will be important to determine whether there are safety concerns associated with chronic TGFβ2/3 inhibition. Intriguingly, recent studies of a TGFβ1-selective inhibitory antibody showed increased anti-tumor immunity but decreased toxicities compared to pan-TGFβ blockade (*66*). These observations suggest that specific pathological processes associated with excessive TGFβ isoform activity may be targeted while sparing the homeostatic roles of other isoforms, which may be explained in part by compensatory activity across isoforms in certain contexts.

Our study has some limitations. First, the effects we observed with TGFβ isoform specific blockade in short-term mouse models may not be recapitulated in established human fibrotic diseases. Pathological features in human diseases are often not fully represented in mouse models, and the therapeutic effects and relative lack of toxicity that we observed in a preventive setting may not translate to long-term intervention in established chronic disease. Second, inhibiting one TGFβ isoform may lead to compensatory effects from other isoforms; this possibility requires further investigation. Finally, although we evaluated global genetic deletion or pharmacologic inhibition of TGFβ2 and 3, we did not assess the in vivo effects of TGFβ isoforms in discrete cell types. Future experiments employing cell-type specific conditional KO mice may help to elucidate more context-specific roles for TGFβ isoforms.

TGFβ has long been implicated as a key mediator of pathological fibrosis but its multifarious homeostatic functions have presented challenges to developing therapeutic TGFβ inhibitors with an acceptable therapeutic index. Although the three TGFβ isoforms are capable of mediating similar signaling activities on target cells, their divergent LAP domains and expression patterns implicate unique roles for each isoform, supported by genetic loss-of-function evidence in mice and humans. In this study, we show that the thresholds for and mechanisms of activation of latent TGFβ2 and TGFβ3 are distinct from those of TGFβ1. Unlike TGFβ1, TGFβ2 and TGFβ3 exhibit increased expression in human fibrotic tissue and in mouse models of lung and liver fibrosis; and isoform-selective therapeutic inhibition of TGFβ2 and TGFβ3 with a potent allosteric antibody can ameliorate experimental fibrosis in vivo. These findings support isoform-selective TGFβ2 and/or TGFβ3 inhibition as a therapeutic strategy for patients with chronic fibrotic disorders.

MATERIALS AND METHODS

Study design

The study aimed to understand the activation mechanisms of different TGFβ isoforms and determine whether TGFβ2 and TGFβ3 play important roles during fibrogenesis in vivo. TGFβ in vitro activities were assessed by TGFβ-responsive reporter assays. Full-length TGFβ proteins were generated either by transient transfection or as recombinant Fc fusion proteins. To investigate the effects of TGFβ2 and/or TGFβ3 in mouse fibrosis models, isoform specific monoclonal antibodies and conditional knock-out mice were generated. Profibrotic gene expression, hydroxyproline, and histology in mouse samples were analyzed to assess the severity of fibrosis. Study sizes and end points were selected on the basis of previous experience with the respective animal models. Animals were randomly assigned to treatment groups. Biological replicates used different animals, sex- and age-matched compared across groups. Experimental group sizes (n) are stated in the figure legends. No data were excluded. Investigators were not blinded when performing and analyzing the data. Three or more independent experiments were performed in each case. All animal experiments were approved by the Institutional Animal Care and Use Committee at Genentech, Inc.

Statistical analysis

Data are expressed as the Mean ± S.E.M. in the main text. Data and statistical analyses were done with Prism 8 (GraphPad Software). Variable differences between experimental and control groups were assessed using the Student's *t*-tests. One-way ANOVA followed by Dunnett's test were used for comparisons of multiple treatment groups with the control group. P-values were used to determine statistical significance and are shown in figure legends.

SUPPLEMENTARY MATERIALS:

Materials and Methods

Fig. S1. Alignment of human TGFβ isoform sequences.

Fig. S2. Characterization of FL-TGFβ1, FL-TGFβ2 and FL-TGFβ3.

Fig. S3. Cellular composition and TGFβ3 expression in IPF lung samples.

Fig. S4. TGFβ2 and TGFβ3 expression in bleomycin-challenged mouse lung.

Fig. S5. Schematics of TGFβ2 and TGFβ3 conditional knockout.

Fig. S6. 6F12 and 4A11 inhibited mouse and human TGFβ2 comparably.

Fig. S7. Surface plasmon resonance sensorgrams for binding of the TGFβR2 to TGFβ ligands in the presence of anti-TGFβ antibodies.

Fig. S8. 4A11 binds to a different epitope of TGFβ2 than the TGFβR complex.

Fig. S9. TGFβ2 and TGFβ3 blockade does not lead to enhanced immune responses that are associated with the pan anti-TGFβ antibody treatment.

Table S1. Characteristics of isoform-selective anti-TGFβ monoclonal antibodies.

Table S2. Characteristics of humanized 4A11 clone.

Table S3. Data collection and refinement statistics for TGFβ2/4A11 structures.

Table S4. Amino acids in the 4A11 epitope interacting with TGFβ2 dimers.

Table S5. Primary amino acid sequences at various positions among TGFβ1, β2, β3 that interact with the 4A11 epitope.

Table S6. Anti-TGFβ isoform-specific antibodies all exhibited favorable pharmacokinetics in C57BL/6 mice.

Data file S1. raw data.

REFERENCES AND NOTES:

1. I. E. Fernandez, O. Eickelberg, The impact of TGF-beta on lung fibrosis: from targeting to biomarkers. *Proc Am Thorac Soc* **9**, 111-116 (2012).
2. S. Dooley, P. ten Dijke, TGF-beta in progression of liver disease. *Cell Tissue Res* **347**, 245-256 (2012).
3. R. Lafyatis, Transforming growth factor beta--at the centre of systemic sclerosis. *Nature reviews. Rheumatology* **10**, 706-719 (2014).
4. J. S. Munger, D. Sheppard, Cross talk among TGF-beta signaling pathways, integrins, and the extracellular matrix. *Cold Spring Harbor perspectives in biology* **3**, a005017 (2011).
5. R. Derynck, E. H. Budi, Specificity, versatility, and control of TGF-beta family signaling. *Science signaling* **12**, (2019).
6. M. M. Shull *et al.*, Targeted disruption of the mouse transforming growth factor-beta 1 gene results in multifocal inflammatory disease. *Nature* **359**, 693-699 (1992).
7. A. B. Kulkarni *et al.*, Transforming growth factor beta 1 null mutation in mice causes excessive inflammatory response and early death. *Proceedings of the National Academy of Sciences of the United States of America* **90**, 770-774 (1993).
8. L. P. Sanford *et al.*, TGFbeta2 knockout mice have multiple developmental defects that are non-overlapping with other TGFbeta knockout phenotypes. *Development* **124**, 2659-2670 (1997).
9. V. Kaartinen *et al.*, Abnormal lung development and cleft palate in mice lacking TGF-beta 3 indicates defects of epithelial-mesenchymal interaction. *Nature genetics* **11**, 415-421 (1995).
10. G. Proetzel *et al.*, Transforming growth factor-beta 3 is required for secondary palate fusion. *Nature genetics* **11**, 409-414 (1995).

11. L. Yaswen *et al.*, Autoimmune manifestations in the transforming growth factor-beta 1 knockout mouse. *Blood* **87**, 1439-1445 (1996).
12. M. J. Anderton *et al.*, Induction of heart valve lesions by small-molecule ALK5 inhibitors. *Toxicol Pathol* **39**, 916-924 (2011).
13. K. Frazier *et al.*, Inhibition of ALK5 signaling induces physeal dysplasia in rats. *Toxicol Pathol* **35**, 284-295 (2007).
14. M. S. Mitra *et al.*, A Potent Pan-TGFbeta Neutralizing Monoclonal Antibody Elicits Cardiovascular Toxicity in Mice and Cynomolgus Monkeys. *Toxicological sciences : an official journal of the Society of Toxicology* **175**, 24-34 (2020).
15. C. E. Barkauskas *et al.*, Type 2 alveolar cells are stem cells in adult lung. *The Journal of clinical investigation* **123**, 3025-3036 (2013).
16. T. Sun *et al.*, TAZ is required for lung alveolar epithelial cell differentiation after injury. *JCI Insight* **5**, (2019).
17. A. K. Wheaton *et al.*, The vitronectin RGD motif regulates TGF-beta-induced alveolar epithelial cell apoptosis. *American journal of physiology. Lung cellular and molecular physiology* **310**, L1206-1217 (2016).
18. A. Sureshbabu *et al.*, Conditional overexpression of TGFbeta1 promotes pulmonary inflammation, apoptosis and mortality via TGFbetaR2 in the developing mouse lung. *Respiratory research* **16**, 4 (2015).
19. M. Abe *et al.*, An assay for transforming growth factor-beta using cells transfected with a plasminogen activator inhibitor-1 promoter-luciferase construct. *Anal Biochem* **216**, 276-284 (1994).
20. S. Li, X. Gu, S. Yi, The Regulatory Effects of Transforming Growth Factor-beta on Nerve Regeneration. *Cell transplantation* **26**, 381-394 (2017).

21. P. D. Brown, L. M. Wakefield, A. D. Levinson, M. B. Sporn, Physicochemical activation of recombinant latent transforming growth factor-beta's 1, 2, and 3. *Growth factors* **3**, 35-43 (1990).

22. J. S. Munger *et al.*, The integrin alpha v beta 6 binds and activates latent TGF beta 1: a mechanism for regulating pulmonary inflammation and fibrosis. *Cell* **96**, 319-328 (1999).

23. C. M. Dubois *et al.*, Evidence that furin is an authentic transforming growth factor-beta1-converting enzyme. *The American journal of pathology* **158**, 305-316 (2001).

24. E. P. Bottinger *et al.*, The recombinant proregion of transforming growth factor beta1 (latency-associated peptide) inhibits active transforming growth factor beta1 in transgenic mice. *Proceedings of the National Academy of Sciences of the United States of America* **93**, 5877-5882 (1996).

25. D. J. DePianto *et al.*, Heterogeneous gene expression signatures correspond to distinct lung pathologies and biomarkers of disease severity in idiopathic pulmonary fibrosis. *Thorax* **70**, 48-56 (2015).

26. M. A. Mouratis, V. Aidinis, Modeling pulmonary fibrosis with bleomycin. *Current opinion in pulmonary medicine* **17**, 355-361 (2011).

27. M. E. Blaauboer *et al.*, Novel combination of collagen dynamics analysis and transcriptional profiling reveals fibrosis-relevant genes and pathways. *Matrix Biol* **32**, 424-431 (2013).

28. M. Lo *et al.*, Effector-attenuating Substitutions That Maintain Antibody Stability and Reduce Toxicity in Mice. *The Journal of biological chemistry* **292**, 3900-3908 (2017).

29. S. Radaev *et al.*, Ternary complex of transforming growth factor-beta1 reveals isoform-specific ligand recognition and receptor recruitment in the superfamily. *The Journal of biological chemistry* **285**, 14806-14814 (2010).

30. E. del Re, J. L. Babitt, A. Pirani, A. L. Schneyer, H. Y. Lin, In the absence of type III receptor, the transforming growth factor (TGF)-beta type II-B receptor requires the type I receptor to bind TGF-beta2. *The Journal of biological chemistry* **279**, 22765-22772 (2004).

31. A. Moulin *et al.*, Structures of a pan-specific antagonist antibody complexed to different isoforms of TGFbeta reveal structural plasticity of antibody-antigen interactions. *Protein science : a publication of the Protein Society* **23**, 1698-1707 (2014).

32. C. Grutter *et al.*, A cytokine-neutralizing antibody as a structural mimetic of 2 receptor interactions. *Proceedings of the National Academy of Sciences of the United States of America* **105**, 20251-20256 (2008).

33. J. Groppe *et al.*, Cooperative assembly of TGF-beta superfamily signaling complexes is mediated by two disparate mechanisms and distinct modes of receptor binding. *Molecular cell* **29**, 157-168 (2008).

34. S. K. Murphy *et al.*, Relationship between methylome and transcriptome in patients with nonalcoholic fatty liver disease. *Gastroenterology* **145**, 1076-1087 (2013).

35. C. A. Moylan *et al.*, Hepatic gene expression profiles differentiate presymptomatic patients with mild versus severe nonalcoholic fatty liver disease. *Hepatology* **59**, 471-482 (2014).

36. J. C. Marie, D. Liggitt, A. Y. Rudensky, Cellular mechanisms of fatal early-onset autoimmunity in mice with the T cell-specific targeting of transforming growth factor-beta receptor. *Immunity* **25**, 441-454 (2006).

37. M. O. Li, S. Sanjabi, R. A. Flavell, Transforming growth factor-beta controls development, homeostasis, and tolerance of T cells by regulatory T cell-dependent and -independent mechanisms. *Immunity* **25**, 455-471 (2006).

38. M. C. Kullberg *et al.*, Helicobacter hepaticus triggers colitis in specific-pathogen-free interleukin-10 (IL-10)-deficient mice through an IL-12- and gamma interferon-dependent mechanism. *Infection and immunity* **66**, 5157-5166 (1998).

39. M. C. Kullberg *et al.*, Helicobacter hepaticus-induced colitis in interleukin-10-deficient mice: cytokine requirements for the induction and maintenance of intestinal inflammation. *Infection and immunity* **69**, 4232-4241 (2001).

40. M. C. Kullberg *et al.*, IL-23 plays a key role in Helicobacter hepaticus-induced T cell-dependent colitis. *The Journal of experimental medicine* **203**, 2485-2494 (2006).

41. J. P. Annes, J. S. Munger, D. B. Rifkin, Making sense of latent TGFbeta activation. *J Cell Sci* **116**, 217-224 (2003).

42. C. Querfeld, B. Eckes, C. Huerkamp, T. Krieg, S. Sollberg, Expression of TGF-beta 1, -beta 2 and -beta 3 in localized and systemic scleroderma. *Journal of dermatological science* **21**, 13-22 (1999).

43. J. Y. Shin *et al.*, Epigenetic activation and memory at a TGFB2 enhancer in systemic sclerosis. *Science translational medicine* **11**, (2019).

44. A. Dropmann *et al.*, TGF-beta1 and TGF-beta2 abundance in liver diseases of mice and men. *Oncotarget* **7**, 19499-19518 (2016).

45. M. A. Burke *et al.*, Molecular profiling of dilated cardiomyopathy that progresses to heart failure. *JCI Insight* **1**, (2016).

46. N. C. Henderson *et al.*, Targeting of alphav integrin identifies a core molecular pathway that regulates fibrosis in several organs. *Nature medicine* **19**, 1617-1624 (2013).

47. N. I. Reed *et al.*, The alphavbeta1 integrin plays a critical in vivo role in tissue fibrosis. *Science translational medicine* **7**, 288ra279 (2015).

48. K. K. Kim, D. Sheppard, H. A. Chapman, TGF-beta1 Signaling and Tissue Fibrosis. *Cold Spring Harbor perspectives in biology* **10**, (2018).
49. K. Miyazono, Positive and negative regulation of TGF-beta signaling. *J Cell Sci* **113 (Pt 7)**, 1101-1109 (2000).
50. A. P. Hinck, T. D. Mueller, T. A. Springer, Structural Biology and Evolution of the TGF-beta Family. *Cold Spring Harbor perspectives in biology* **8**, (2016).
51. M. Shi *et al.*, Latent TGF-beta structure and activation. *Nature* **474**, 343-349 (2011).
52. M. E. Lindsay *et al.*, Loss-of-function mutations in TGFB2 cause a syndromic presentation of thoracic aortic aneurysm. *Nature genetics* **44**, 922-927 (2012).
53. A. M. Bertoli-Avella *et al.*, Mutations in a TGF-beta ligand, TGFB3, cause syndromic aortic aneurysms and dissections. *J Am Coll Cardiol* **65**, 1324-1336 (2015).
54. D. Schepers *et al.*, A mutation update on the LDS-associated genes TGFB2/3 and SMAD2/3. *Human mutation* **39**, 621-634 (2018).
55. L. Gorelik, R. A. Flavell, Abrogation of TGFbeta signaling in T cells leads to spontaneous T cell differentiation and autoimmune disease. *Immunity* **12**, 171-181 (2000).
56. D. H. Kaplan *et al.*, Autocrine/paracrine TGFbeta1 is required for the development of epidermal Langerhans cells. *The Journal of experimental medicine* **204**, 2545-2552 (2007).
57. M. O. Li, Y. Y. Wan, R. A. Flavell, T cell-produced transforming growth factor-beta1 controls T cell tolerance and regulates Th1- and Th17-cell differentiation. *Immunity* **26**, 579-591 (2007).

58. A. Bobr *et al.*, Autocrine/paracrine TGF-beta1 inhibits Langerhans cell migration. *Proceedings of the National Academy of Sciences of the United States of America* **109**, 10492-10497 (2012).

59. H. Ishigame *et al.*, Excessive Th1 responses due to the absence of TGF-beta signaling cause autoimmune diabetes and dysregulated Treg cell homeostasis. *Proceedings of the National Academy of Sciences of the United States of America* **110**, 6961-6966 (2013).

60. X. Yu *et al.*, The Cytokine TGF-beta Promotes the Development and Homeostasis of Alveolar Macrophages. *Immunity* **47**, 903-912 e904 (2017).

61. N. Takeda *et al.*, TGF-beta Signaling-Related Genes and Thoracic Aortic Aneurysms and Dissections. *International journal of molecular sciences* **19**, (2018).

62. B. L. Loeys *et al.*, A syndrome of altered cardiovascular, craniofacial, neurocognitive and skeletal development caused by mutations in TGFBR1 or TGFBR2. *Nature genetics* **37**, 275-281 (2005).

63. K. Janssens *et al.*, Mutations in the gene encoding the latency-associated peptide of TGF-beta 1 cause Camurati-Engelmann disease. *Nature genetics* **26**, 273-275 (2000).

64. M. E. Lacouture *et al.*, Cutaneous keratoacanthomas/squamous cell carcinomas associated with neutralization of transforming growth factor beta by the monoclonal antibody fresolimumab (GC1008). *Cancer Immunol Immunother* **64**, 437-446 (2015).

65. L. M. Rice *et al.*, Fresolimumab treatment decreases biomarkers and improves clinical symptoms in systemic sclerosis patients. *The Journal of clinical investigation* **125**, 2795-2807 (2015).

66. C. J. Martin *et al.*, Selective inhibition of TGFbeta1 activation overcomes primary resistance to checkpoint blockade therapy by altering tumor immune landscape. *Science translational medicine* **12**, (2020).

67. J. Seibler *et al.*, Rapid generation of inducible mouse mutants. *Nucleic acids research* **31**, e12 (2003).

68. M. A. van Waarde, A. J. van Assen, H. H. Kampinga, A. W. Konings, Z. Vujaskovic, Quantification of transforming growth factor-beta in biological material using cells transfected with a plasminogen activator inhibitor-1 promoter-luciferase construct. *Anal Biochem* **247**, 45-51 (1997).

69. S. A. Khan, J. Joyce, T. Tsuda, Quantification of active and total transforming growth factor-beta levels in serum and solid organ tissues by bioassay. *BMC research notes* **5**, 636 (2012).

70. A. Moeller, K. Ask, D. Warburton, J. Gauldie, M. Kolb, The bleomycin animal model: a useful tool to investigate treatment options for idiopathic pulmonary fibrosis? *The international journal of biochemistry & cell biology* **40**, 362-382 (2008).

71. J. L. Gardner *et al.*, Measurement of liver collagen synthesis by heavy water labeling: effects of profibrotic toxicants and antifibrotic interventions. *Am J Physiol Gastrointest Liver Physiol* **292**, G1695-1705 (2007).

72. A. J. McCoy, R. W. Grosse-Kunstleve, L. C. Storoni, R. J. Read, Likelihood-enhanced fast translation functions. *Acta crystallographica. Section D, Biological crystallography* **61**, 458-464 (2005).

73. L. Del Amo-Maestro, L. Marino-Puertas, T. Goulas, F. X. Gomis-Ruth, Recombinant production, purification, crystallization, and structure analysis of human transforming growth factor beta2 in a new conformation. *Scientific reports* **9**, 8660 (2019).

74. P. D. Adams *et al.*, PHENIX: a comprehensive Python-based system for macromolecular structure solution. *Acta crystallographica. Section D, Biological crystallography* **66**, 213-221 (2010).

75. P. Emsley, K. Cowtan, Coot: model-building tools for molecular graphics. *Acta crystallographica. Section D, Biological crystallography* **60**, 2126-2132 (2004).

76. G. N. Murshudov, A. A. Vagin, E. J. Dodson, Refinement of macromolecular structures by the maximum-likelihood method. *Acta crystallographica. Section D, Biological crystallography* **53**, 240-255 (1997).

77. J. R. Rock *et al.*, Multiple stromal populations contribute to pulmonary fibrosis without evidence for epithelial to mesenchymal transition. *Proceedings of the National Academy of Sciences of the United States of America* **108**, E1475-1483 (2011).

78. T. J. Schall *et al.*, Molecular cloning and expression of a receptor for human tumor necrosis factor. *Cell* **61**, 361-370 (1990).

79. L. E. Gentry *et al.*, Type 1 transforming growth factor beta: amplified expression and secretion of mature and precursor polypeptides in Chinese hamster ovary cells. *Molecular and cellular biology* **7**, 3418-3427 (1987).

80. T. Stuart *et al.*, Comprehensive Integration of Single-Cell Data. *Cell* **177**, 1888-1902 e1821 (2019).

81. R Core Team, R: A language and environment for statistical computing. R Foundation for Statistical Computing, Vienna, Austria. URL https://www.R-project.org. (2020).

82. J. H. Krijthe, Rtsne: T-distributed stochastic neighbor embedding using Barnes-Hut implementation. (2015).

83. X. Y. Zhao, B. E. Wang, X. M. Li, T. L. Wang, Newly proposed fibrosis staging criterion for assessing carbon tetrachloride- and albumin complex-induced liver fibrosis in rodents. *Pathol Int* **58**, 580-588 (2008).

84. S. Seeber *et al.*, A robust high throughput platform to generate functional recombinant monoclonal antibodies using rabbit B cells from peripheral blood. *PloS one* **9**, e86184 (2014).

85. L. D. Goldstein *et al.*, Massively parallel single-cell B-cell receptor sequencing enables rapid discovery of diverse antigen-reactive antibodies. *Communications biology* **2**, 304 (2019).

86. J. R. Dasch, D. R. Pace, W. Waegell, D. Inenaga, L. Ellingsworth, Monoclonal antibodies recognizing transforming growth factor-beta. Bioactivity neutralization and transforming growth factor beta 2 affinity purification. *J Immunol* **142**, 1536-1541 (1989).

87. J. Foote, G. Winter, Antibody framework residues affecting the conformation of the hypervariable loops. *Journal of molecular biology* **224**, 487-499 (1992).

88. Z. Zou, P. D. Sun, An improved recombinant mammalian cell expression system for human transforming growth factor-beta2 and -beta3 preparations. *Protein expression and purification* **50**, 9-17 (2006).

89. Z. Otwinowski, W. Minor, Processing of X-ray diffraction data collected in oscillation mode. *Methods in enzymology* **276**, 307-326 (1997).

Acknowledgements: We thank Brigid Hogan for providing SPC-WT-Tm mice; Karen Billeci, Jackson Egen, and Wenjun Ouyang for support during the early library screening; Shannon Turley for helpful discussions; Kathy Hötzel and Sreedevi Chalasani for developing the dual ISH/IHC staining protocol; Jiabing Ding for cloning various expression plasmids; Changyun Hu for antibody cloning support and Genentech core laboratories for technical assistance. This research used resources of the Advanced Photon Source, a U.S. Department of Energy (DOE) Office of Science User Facility operated for the DOE Office of Science by Argonne National Laboratory under Contract No. DE-AC02-06CH11357. **Funding:** This work was supported by Genentech Inc.

Author contributions: T.S. conceived the project, proposed the therapeutic hypothesis and led the biology studies, designed and performed the library screening, in vitro TGFβ functional characterization, and helped design and perform in vivo experiments and gene expression analysis. Z.H., S.J. performed and C.E., H.D.B. designed and supervised in vivo fibrosis experiments. H.Z. and M.X. designed and performed the colitis study. W.Y.L., J.W., C.H. and D.S. carried out immunization and identified anti-TGFβ antibodies. W.C.L. and Y.W. humanized and engineered antibodies and performed biochemical analysis. J.M.V. and Y.G.M. provided in vitro functional analyses of antibodies. J.L., R.Y. and S.S. designed and analyzed pharmacokinetic data. J.Y. and P.L. generated crystals and solved and analyzed the crystal structure. P.L. designed expression constructs. P.C. provided histology and pathology analysis. E.N.D. cloned and generated MLEC reporters, established the 2-cell reporter assay. J.A.V.H. and A.R.A. provided bioinformatic analyses for human and mouse datasets. T.W., M.W. and R.C. generated and purified proteins and antibodies. D.J.D., K.B.M.,

K.H.S., Z.M. performed human IPF scRNAseq data generation and analysis. P.J.W. provided human IPF lung samples. M.R.G. designed and generated cKO mice. N.G. established and initially characterized TGFβ3.cKO line. T.R.R. performed human gene expression analysis. Y.W. led the molecular characterization of antibodies. T.S. and J.R.A. analyzed the data and wrote the manuscript with help from all authors. J.R.A. is the senior author and supervised the project. **Competing interests:** All authors except P.W. are current or past employees of Genentech, a member of the Roche group, and may hold Roche stock or stock options. A patent application titled "Isoform-selective anti-TGF-beta antibodies and methods of use," relating to the subject matter of this manuscript, has been provisionally filed by Genentech, Inc. **Data and materials availability:** All data associated with this study are in the paper or supplementary materials. RNAseq data on sorted cell populations in the bleomycin model were deposited in the NCBI Gene Expression Omnibus (GEO; https://www.ncbi.nlm.nih.gov/geo) database under accession GSE168529. Single cell RNA-seq data from human IPF lung was deposited under accession GSE159354; specific IPF samples used in this study are under accessions GSM4827158-62, GSM4827186-95, and GSM4827201-05. The atomic coordinates and structure factors for 4A11/TGFβ2 complex structure have been deposited into Protein Data Bank under the access code 6XM2.

FIGURE LEGENDS:

Fig. 1. **Full length TGFβ3 conditioned media inhibits alveolosphere formation in vitro.** (**A**) Schematic of the expression plasmid library screening using alveolar organoid culture: TdTomato^{+} lineage labeled AEC2s were cultured in Matrigel with NHLF for 2 weeks or until alveolospheres develop in the conditioned media from transfections. (**B** to **G**) Fluorescence full plate images show the alveolospheres at end of the culture with the conditioned media from transfections with (B) a control plasmid, (C) FL-TGFβ1 expression construct, (D) FL-TGFβ3 expression construct, or cultured with recombinant proteins, (E) none, (F) TGFβ1 mature peptide (10ng/ml), or (G) TGFβ3 mature peptide (10ng/ml). Scale bar, 1mm. Experiments were repeated > 3 times. (**H**) Schematic of TGFβ constructs. Intracellular furin cleavage of a full length TGFβ propeptide yields a non-covalently associated LAP and receptor-binding domain forming FL-TGFβ in conditioned media. Recombinant mature TGFβ lacks the LAP domain.

Fig. 2. Full-length TGFβ2 and TGFβ3 can "intrinsically" activate TGFβR-dependent signaling. (**A**) Schematic of 2-cell integrin-dependent TGFβ reporter assay. (**B**) 293T cells were transfected with a plasmid encoding FL-TGFβ1or FL-TGFβ3 (wild-type or RGE mutants) with or without plasmids encoding integrins αv and β6 and co-cultured with MLEC reporter cells. The percentages of increase by integrin mediated activation are shown. (**C**) Supernatants (SN) were collected from cells transfected with a plasmid encoding FL-TGFβ1, FL-TGFβ2, FL-TGFβ3 or an empty vector (control). Supernatants were acidified as indicated (HCl treatment). TGFβ activities were measured in MLEC reporter cells. (**D**) TGFβ activities were measured in MLEC reporter cells after incubation with a series of concentrations of human Fc-FL-TGFβ isoform fusion proteins. Background, no fusion protein added. (**E**) Human Fc-FL-TGFβ2 or Fc-FL-TGFβ3 fusion proteins (30ng/ml) were incubated with isoform specific antibodies:

namely, 19D8 (anti-TGFβ1); 6F12 (anti-TGFβ2); 2A10 (anti-TGFβ3); and 1D11 (pan-anti-TGFβ) at 3μg/ml, and TGFβ activity was measured with MLEC reporter cells. Background, no fusion protein added; none, no antibody added. (**F** to **I**) Mature peptide (1ng/ml) of TGFβ1 (G), TGFβ2 (H) or TGFβ3 (I) was incubated with a series concentrations of human Fc-LAP fusion proteins and TGFβ activity was measured with MLEC reporter cells. Curves are best fit to dose-response inhibition model. IC_{50}s and 95% Confidence Intervals were determined based on the titration curves and are shown in (F). Background, no mature peptide added. (B-E, G-I) Data are averages ± SEM from experiments run in triplicate and error bars are not shown when they are shorter than sizes of their corresponding symbols. (B-E) **, $P < 0.01$; ***, $P < 10^{-3}$; ****, $P < 10^{-4}$; NS, $P > 0.05$ by unpaired two-tailed Student's *t*-test.

Fig. 3. The expression of TGFβ2 and TGFβ3 are elevated in human IPF patient samples. (**A**) Relative gene expression of TGFβ isoforms in non-diseased control (N = 8) and IPF (N = 40) human lung tissue were determined using microarrays from (*25*). Data represent means ± SEM. **, $P < 0.01$; ****, $P < 10^{-4}$; NS, $P > 0.05$ by unpaired two-tailed Student's *t*-test. (**B**) Representative pSMAD2/3 immunohistochemistry (IHC) of normal control and IPF lung tissues, showing nuclear pSMAD staining in fibroblastic foci (enlarged in inset) of IPF lung tissue. Scale bars, 90μm. (**C**) t-SNE plot representing scRNAseq of IPF lungs (N=4, combined) shows representation of multiple cell lineages as labeled in the multi-color master plot. (**D**) Expression (≥ 1 UMI) of individual TGFβ isoforms and TGFβ target genes *SERPINE1* and *COL1A1* are shown on smaller t-SNE plots with the red color denoting detected expression. Box plots show the percent of cells within each major population expressing the given gene, with individual patient sample values denoted by diamonds. (**E**) Dual IHC staining for pSMAD3 (teal) and in situ hybridization (ISH) for TGFβ3 (magenta) shows colocalization of TGFβ3 mRNA and nuclear pSMAD3 in multiple cells in a fibroblastic focus in IPF lung tissue.

Fig. 4. TGFβ2 and TGFβ3 contribute to lung fibrosis in the bleomycin challenge model. (**A** and **B**) Whole lung relative gene expression of TGFβ isoforms (A) and TGFβ targeted genes, *Serpine1*, *Fn1* and *Col1a1* (B) were determined at the indicated timepoints (N=8 per group) after IT bleomycin instillation using microarrays in (*27*). *, P < 0.05; **, P < 0.01; ***, P < 10^{-3}; ****, P < 10^{-4} by unpaired two-tailed Student's *t*-test. Data represent means ± SEM. (**C**) Schematics for in vivo I.T. bleomycin experiments to assess either cKO mice (D and E), or anti-TGFβ antibody treatments (Fig. 6). Deuterated drinking water was provided to animals from day 9-23 to assess the fraction of new collagen production during that interval. Profibrotic lung gene expression were measured at d14 and lung hydroxyproline were measured at d24 after bleomycin administration. (**D** and **E**) Percentages of new hydroxyproline (mean ± SEM) were measured as an indicator of newly synthesized collagen in WT or TGFβ isoform CKO mice. (D) n= 5 (each saline group), n = 20 (WT, BLM), n = 24 mice (β2.cKO, BLM); (E) n = 7 (WT, saline), n = 14 (WT, BLM), n = 13 (β3.cKO, BLM) and n= 13 (β2/3.cDKO, BLM). *P < 0.05, ***P < 0.001 by One-way ANOVA with Dunnett's test.

Fig. 5. Crystal structure reveals an allosteric mechanism of TGFβ inhibition by the anti-TGFβ2/3 antibody, 4A11. (**A**) Crystal structure of the 2:2 complex of the TGFβ2 dimer (green) bound by two 4A11 anti-TGFβ Fabs determined at 1.91Å resolution. The asymmetric unit of the crystal as shown contains two copies of the complex. Heavy chain and light chain of 4A11 are shown in dark orange and light orange, respectively. (**B**) Overview of the TGFβ2 epitope bound by 4A11 (Fab not shown for clarity). TGFβ2 residues bound by 4A11 labeled and shown in orange. (**C**) Close-up interface views of the TGFβ2 epitope and the 4A11 CDR region. Key interface residues in TGFβ2 (Red) and 4A11 CDR (black) are indicated. (**D** and **E**) Cartoons show TGFβ2 from the fresolimumab complex (D, from PDB 4KXZ) and conformational changes in

TGFβ2 induced by 4A11 (E). The TGFβ2 dimers are aligned on the monomer on the left, to show the magnitude of the change to the 4A11 bound dimer. (**F**) A cartoon showing TGFβ2 from 4A11 complex (left) and TGFβ3 from TGFβR1/TGFβR2 complex (right, from PDB 2PJY). The α-helix in green responsible for TGFβR1 binding is shifted in one of the TGFβ2 monomers when bound by 4A11. As in Figures D and E, the TGFβ2 dimers shown are aligned on the monomer on the left.

Fig. 6. anti-TGFβ2 and anti-TGFβ3 antibody treatment reduces lung fibrosis in the bleomycin challenge model. (**A** and **B**) Whole lung gene expression of *Serpine1, Fn1* and *Col1a1* were determined by quantitative RT-PCR 14 days after I.T. saline or bleomycin instillation and treatment with isotype control antibody, anti-TGFβ2 antibody (6F12) (A) or anti-TGFβ3 antibody (2A10) (B). (A) n= 5 (Saline), n = 15 (control, BLM) and n = 14 (6F12, BLM); (B) n= 5 (Saline), n = 19 (control, BLM) and n = 20 mice (2A10, BLM). (**C**) Newly synthesized collagen was determined at day 24 after saline (n = 10) or bleomycin installation. Animals were treated with either an isotype control (n = 21), the combination (n = 23) of 6F12 and 2A10, or anti-TGFβ2/3 antibody (4A11). Doses of 4A11 were high (10mg/kg; 3 times/week, n = 23); mid (10mg/kg; 1 time/week, n = 24), or low (2.5 mg/kg; 1 time/week, n = 23), respectively, as indicated. (**D**) Disease scores were determined by pathology analyses (see Methods). Mouse lungs were harvested 24 days after either saline (n=5) or bleomycin instillation, with treatment by either isotype control (n = 7) or 4A11 (high dose, n = 12).
(**E**) Representative mouse lung images of immunohistochemistry staining for collagen III are shown. (A to D) **P* < 0.05, ***P* < 0.01, *** P < 0.001, **** *P*<0.0001, NS, P>0.05 by One-way ANOVA with Dunnett's test.

Fig. 7. TGFβ2 and TGFβ3 are elevated in human NASH livers and anti-TGFβ2/3 antibody reduces CCl_4 induced liver fibrosis. (**A**) Relative gene expression of TGFβ

isoforms in livers from NASH patients with mild fibrosis (F0 and F1) (N = 40) vs. severe fibrosis (F3 and F4) (N = 32) were determined using published datasets (GSE53845). (**B**) Schematics for the in vivo CCl_4 treated liver fibrosis model to assess the efficacy of the anti-TGFβ2/3 antibody (4A11). Profibrotic lung gene expression and pathology scores were measured after 6 weeks of treatment. (**C**) Relative gene expression of TGFβ isoforms in mouse livers were determined by quantitative RT-PCR at 6 weeks after the initiation of vehicle or CCl_4 treatment. N = 8 for both groups. (**D**) Liver gene expression of *Col1a1* and *Col3a1* were determined by quantitative RT-PCR 6 weeks after the initiation of vehicle or CCl_4 treatment. Animals were preventively treated with either isotype control or 4A11. N = 8 for all groups. (**E**) Liver pathology scores were determined by histopathological analysis (see Methods). Mouse livers were harvested 6 weeks after either vehicle or CCl_4 treatment. N = 8 for all groups. (**F**) Representative histologic images of liver sections stained with Masson's trichrome. *, $P < 0.05$; **, $P < 0.01$; ****, $P < 10^{-4}$; NS, $P > 0.05$ by unpaired two-tailed Student's *t*-test (A and B); ***P* < 0.01 by One-way ANOVA with Dunnett's test (C and D). Data represent means ± SEM.

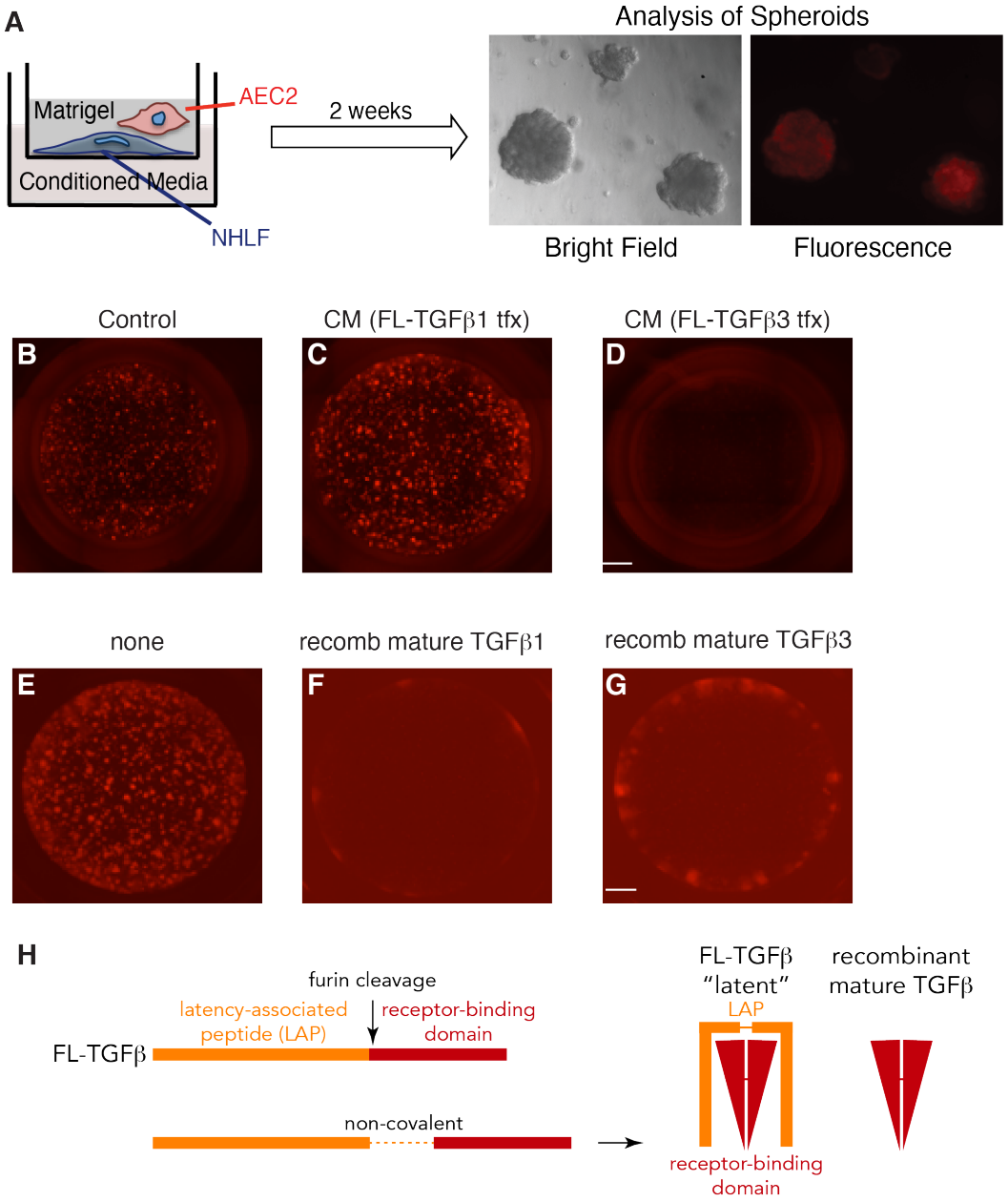
A
Analysis of Spheroids
Matrigel
AEC2
2 weeks
Conditioned Media
NHLF
Bright Field
Fluorescence
Control
CM (FL-TGFβ1 tfx)
CM (FL-TGFβ3 tfx)
B
C
D
none
recomb mature TGFβ1
recomb mature TGFβ3
E
F
G
H
furin cleavage
latency-associated peptide (LAP)
receptor-binding domain
FL-TGFβ
non-covalent
FL-TGFβ "latent"
LAP
recombinant mature TGFβ
receptor-binding domain

Fig. 1

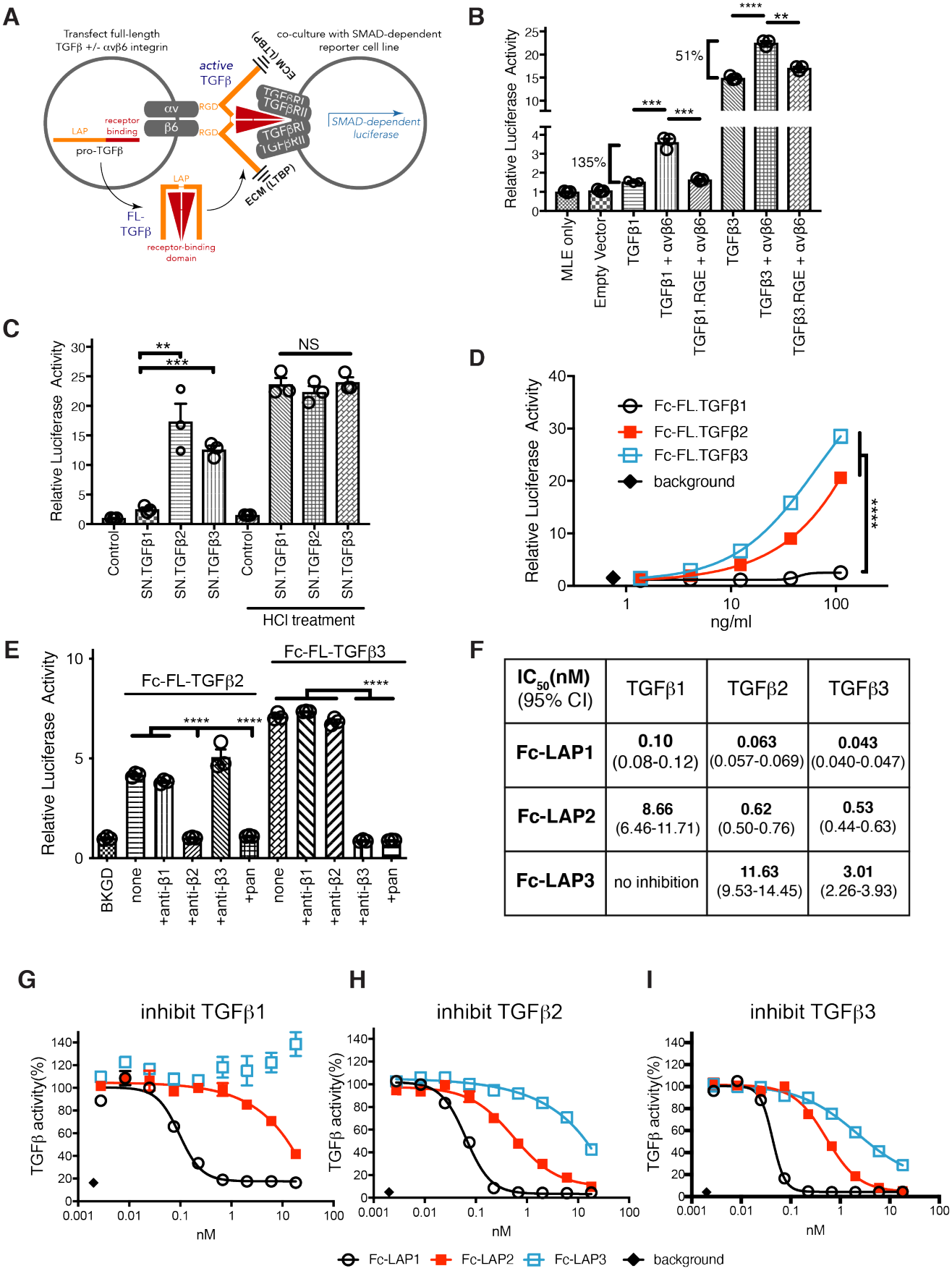

IC_{50}(nM) (95% CI)	TGFβ1	TGFβ2	TGFβ3
Fc-LAP1	**0.10** (0.08-0.12)	**0.063** (0.057-0.069)	**0.043** (0.040-0.047)
Fc-LAP2	**8.66** (6.46-11.71)	**0.62** (0.50-0.76)	**0.53** (0.44-0.63)
Fc-LAP3	no inhibition	**11.63** (9.53-14.45)	**3.01** (2.26-3.93)

Fig. 2

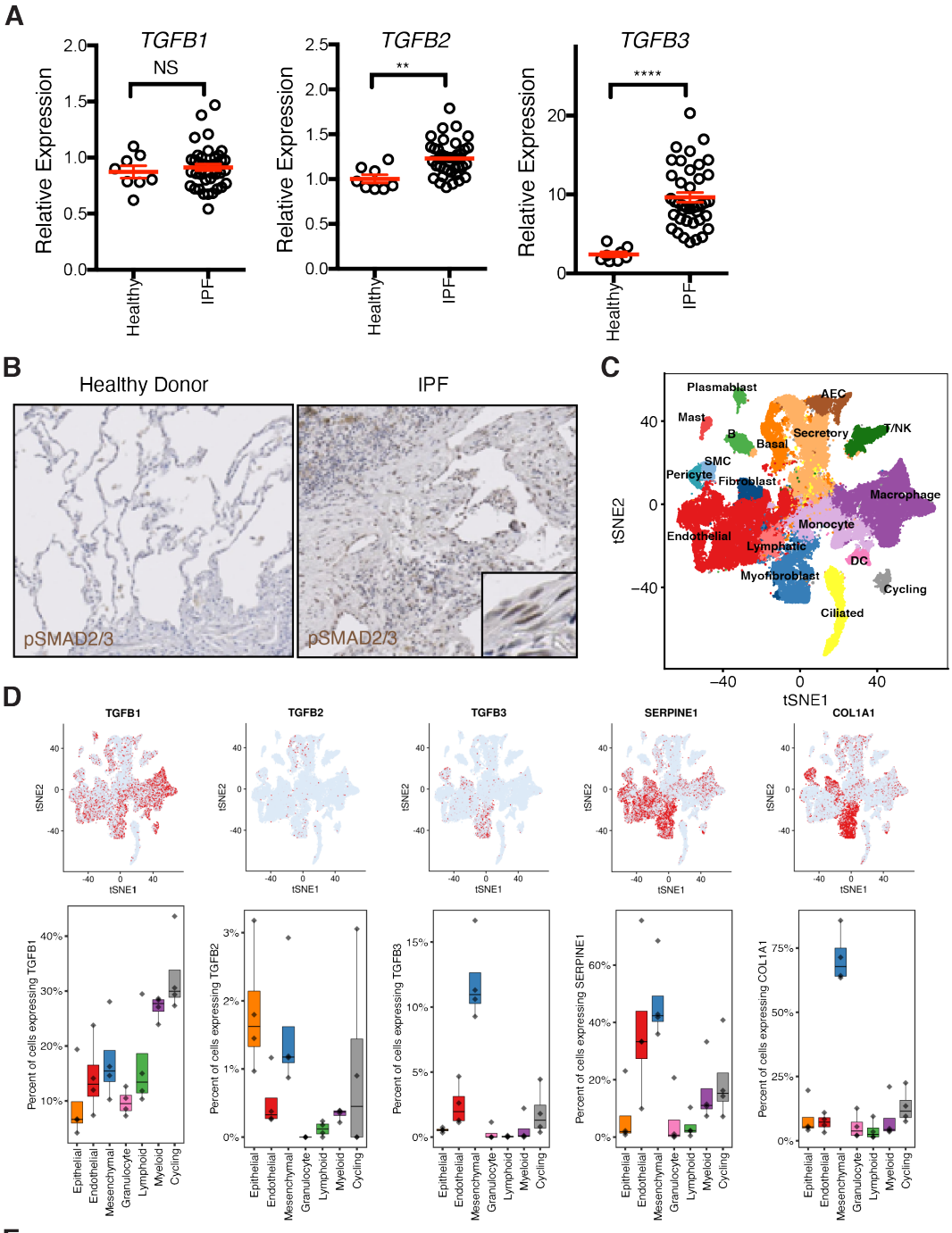
A
TGFB1
NS
TGFB2
**
TGFB3
****
Relative Expression
Healthy
IPF
B
Healthy Donor
IPF
pSMAD2/3
pSMAD2/3
C
Plasmablast
AEC
Mast
B
Secretory
T/NK
Basal
SMC
Pericyte
Fibroblast
Macrophage
Monocyte
Endothelial
Lymphatic
DC
Myofibroblast
Cycling
Ciliated
tSNE1
tSNE2
D
TGFB1
TGFB2
TGFB3
SERPINE1
COL1A1
Percent of cells expressing TGFB1
Percent of cells expressing TGFB2
Percent of cells expressing TGFB3
Percent of cells expressing SERPINE1
Percent of cells expressing COL1A1
Epithelial
Endothelial
Mesenchymal
Granulocyte
Lymphoid
Myeloid
Cycling
E
TGFB3 pSMAD3
20 µm

Fig. 3

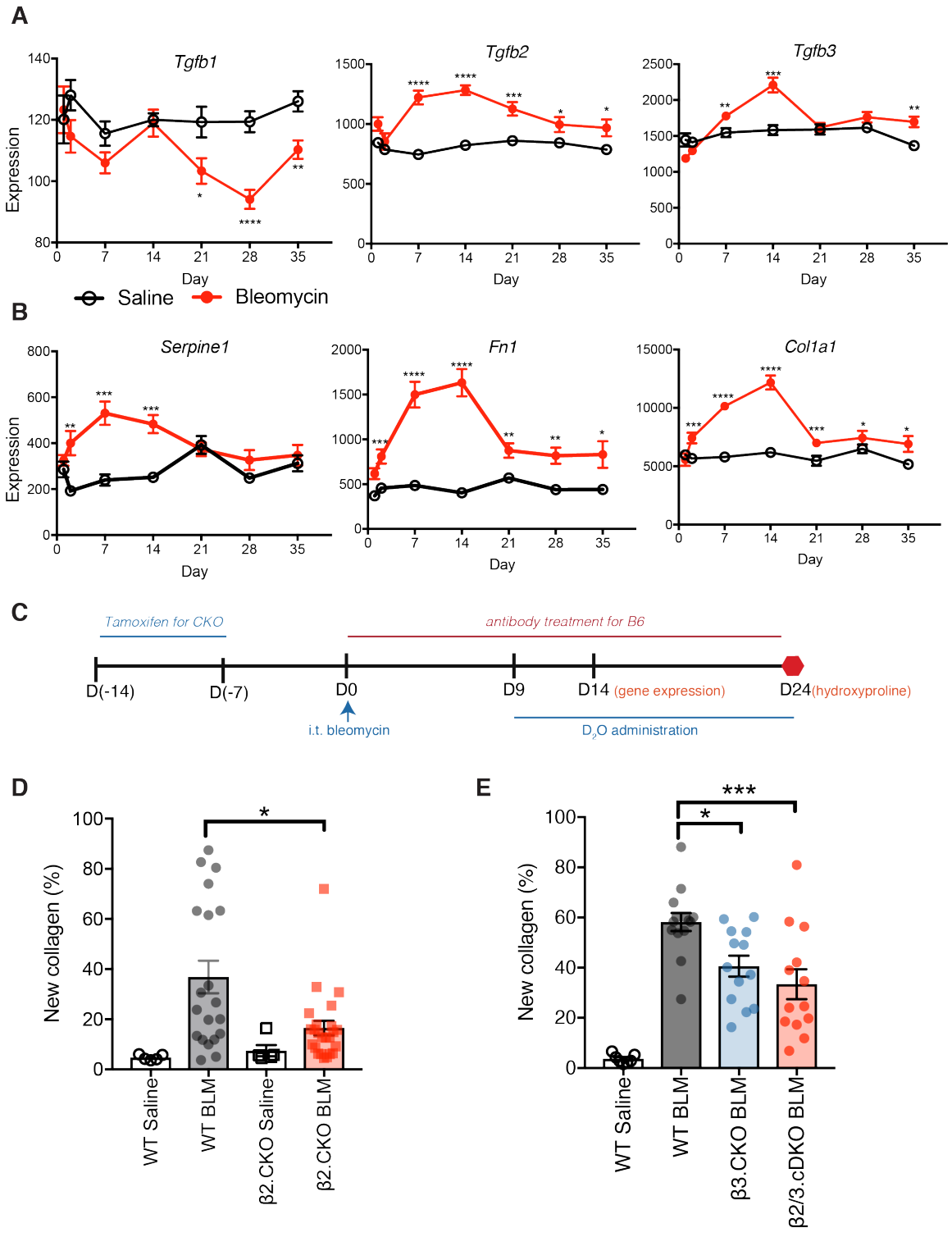
A
Tgfb1
Tgfb2
Tgfb3
Expression
Day
Saline
Bleomycin
B
Serpine1
Fn1
Col1a1
C
Tamoxifen for CKO
antibody treatment for B6
D(-14)
D(-7)
D0
D9
D14 (gene expression)
D24(hydroxyproline)
i.t. bleomycin
D2O administration
D
New collagen (%)
WT Saline
WT BLM
β2.CKO Saline
β2.CKO BLM
E
β3.CKO BLM
β2/3.cDKO BLM

Fig. 4

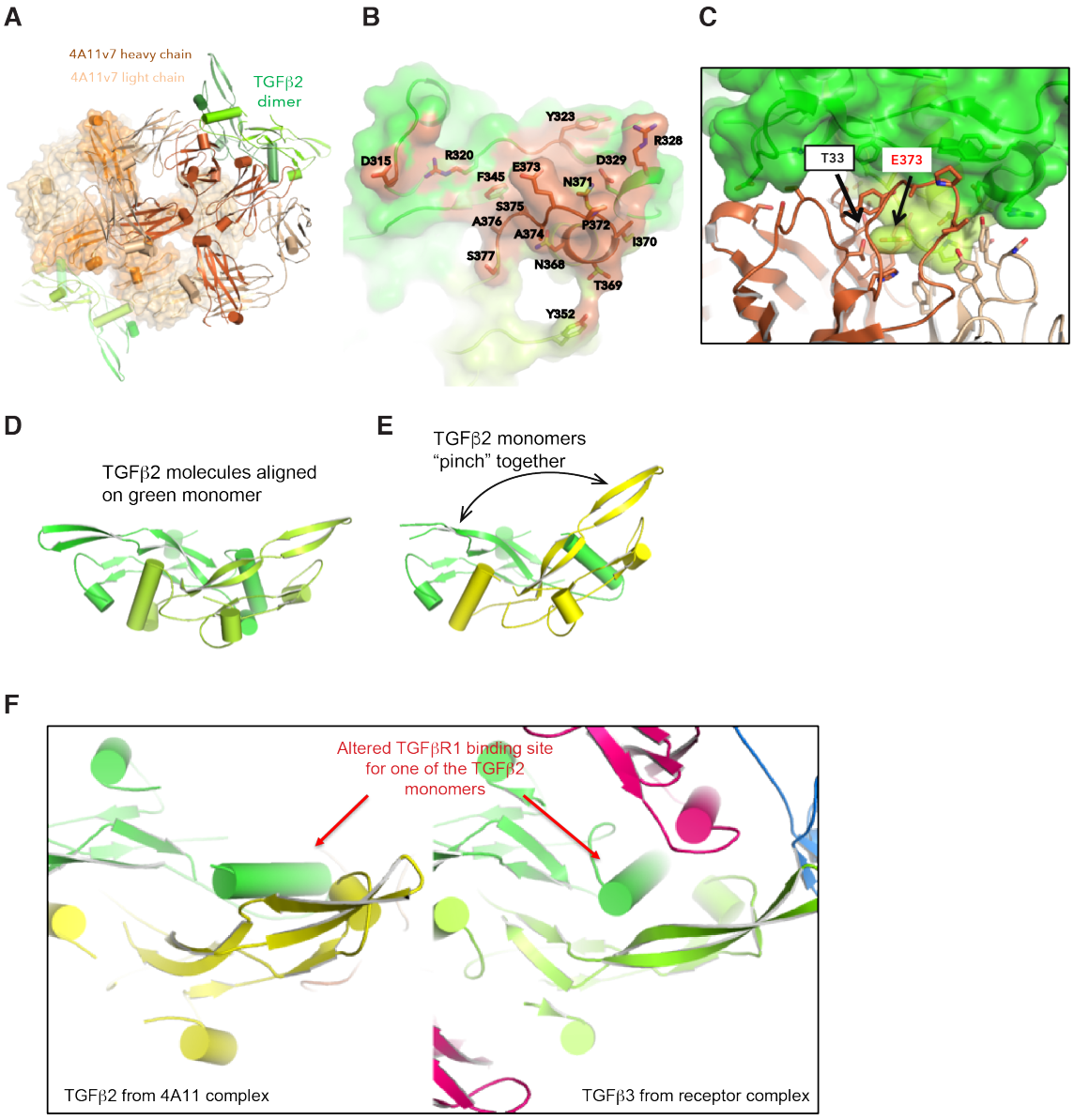
A
4A11v7 heavy chain
4A11v7 light chain
TGFβ2
dimer
B
Y323
R328
D315
R320
D329
F345
E373
N371
S375
A376
A374
P372
I370
S377
N368
T369
Y352
C
T33
E373
D
TGFβ2 molecules aligned
on green monomer
E
TGFβ2 monomers
“pinch” together
F
Altered TGFβR1 binding site
for one of the TGFβ2
monomers
TGFβ2 from 4A11 complex
TGFβ3 from receptor complex

Fig. 5

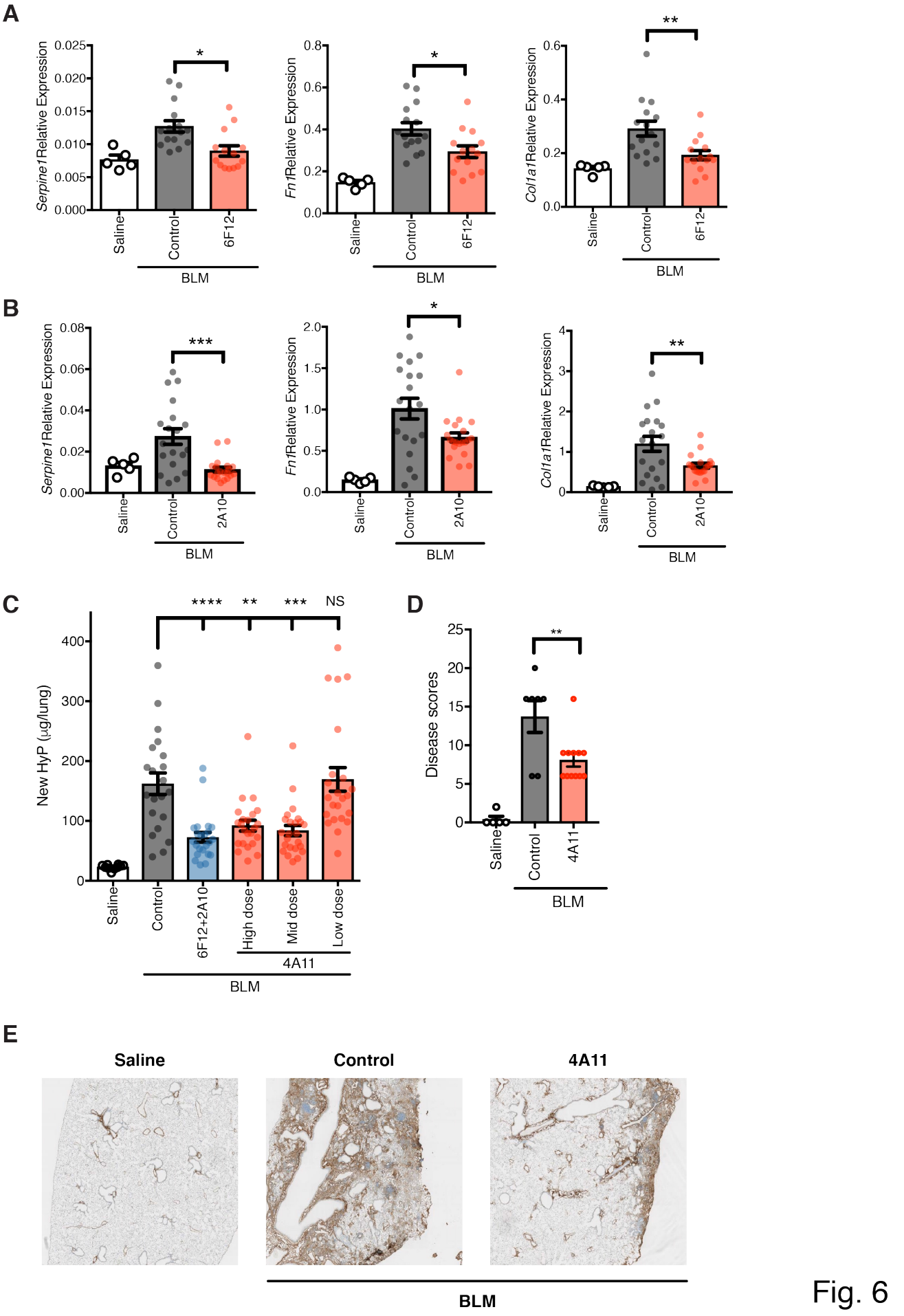
A
Serpine1 Relative Expression
0.025
0.020
0.015
0.010
0.005
0.000
*
Saline
Control
6F12
BLM
Fn1 Relative Expression
0.8
0.6
0.4
0.2
0.0
*
Saline
Control
6F12
BLM
Col1a1 Relative Expression
0.6
0.4
0.2
0.0
**
Saline
Control
6F12
BLM
B
Serpine1 Relative Expression
0.08
0.06
0.04
0.02
0.00
***
Saline
Control
2A10
BLM
Fn1 Relative Expression
2.0
1.5
1.0
0.5
0.0
*
Saline
Control
2A10
BLM
Col1a1 Relative Expression
4
3
2
1
0
**
Saline
Control
2A10
BLM
C
New HyP (μg/lung)
400
300
200
100
0
**** ** *** NS
Saline
Control
6F12+2A10
High dose
Mid dose
Low dose
4A11
BLM
D
Disease scores
25
20
15
10
5
0
**
Saline
Control
4A11
BLM
E
Saline
Control
4A11
BLM

Fig. 6

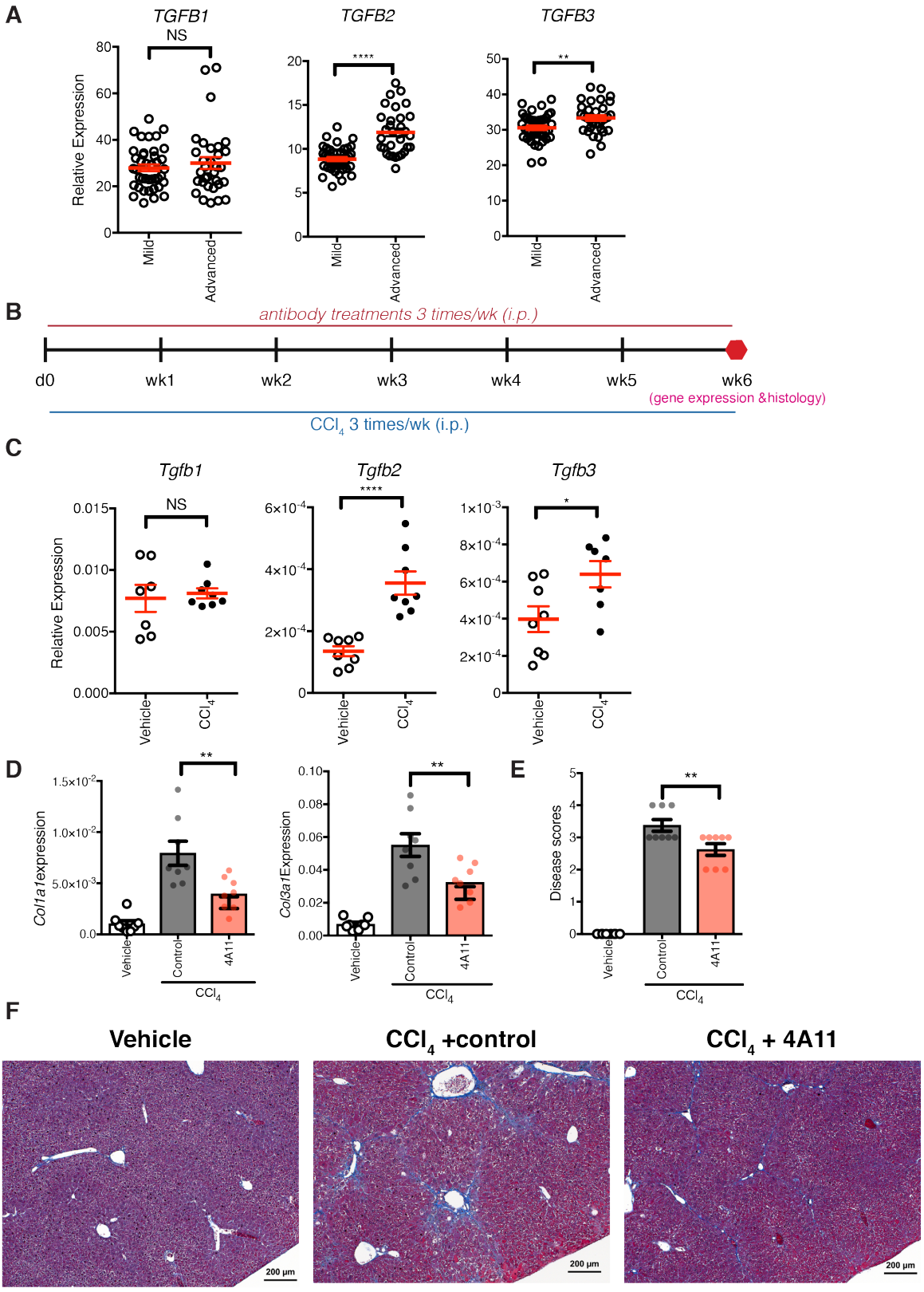
A
TGFB1
TGFB2
TGFB3
NS
****
**
Relative Expression
Mild
Advanced
B
antibody treatments 3 times/wk (i.p.)
d0
wk1
wk2
wk3
wk4
wk5
wk6
(gene expression &histology)
CCl4 3 times/wk (i.p.)
C
Tgfb1
Tgfb2
Tgfb3
NS
****
*
Relative Expression
Vehicle
CCl4
D
Col1a1expression
Col3a1Expression
**
Vehicle
Control
4A11
CCl4
E
Disease scores
**
F
Vehicle
CCl4 +control
CCl4 + 4A11
200 µm

Fig. 7

TGFβ2 and TGFβ3 isoforms drive fibrotic disease pathogenesis

Tianhe Sun[1,*], Zhiyu Huang[2], Wei-Ching Liang[3], Jianping Yin[4], Wei Yu Lin[3], Jia Wu[3], Jean-Michel Vernes[5], Jeff Lutman[6], Patrick Caplazi[7], Surinder Jeet[2], Tiffany Wong[4], Manda Wong[4], Daryle J. DePianto[1], Katrina B. Morshead[1], Kai-Hui Sun[8], Zora Modrusan[8], Jason A. Vander Heiden[9], Alexander R. Abbas[9], Hua Zhang[2], Min Xu[2], Elsa-Noah N'Diaye[1], Meron Roose-Girma[10], Paul J. Wolters[11], Rajbharan Yadav[6], Siddharth Sukumaran[6], Nico Ghilardi[1], Racquel Corpuz[4], Claire Emson[2], Y. Gloria Meng[5], Thirumalai R. Ramalingam[12], Patrick Lupardus[4], Hans D. Brightbill[2], Dhaya Seshasayee[3], Yan Wu[3] and Joseph R. Arron[1,*]

Affiliations:

[1]Department of Immunology Discovery, Genentech, 1 DNA Way, South San Francisco, CA 94080, USA.

[2]Department of Translational Immunology, Genentech, 1 DNA Way, South San Francisco, CA 94080, USA.

[3]Department of Antibody Engineering, Genentech, 1 DNA Way, South San Francisco, CA 94080, USA.

[4]Department of Structural Biology, Genentech, Inc., 1 DNA Way, South San Francisco, CA 94080, USA.

[5]Department of Biochemical and Cellular Pharmacology, Genentech, 1 DNA Way, South San Francisco, CA 94080, USA.

[6]Department of Preclinical and Translational Pharmacokinetics, Genentech, 1 DNA Way, South San Francisco, CA 94080, USA.

[7]Department of Pathology, Genentech, Inc., 1 DNA Way, South San Francisco, CA 94080, USA.

[8]Department of Protein Sciences, Genentech, Inc., 1 DNA Way, South San Francisco, CA 94080, USA.

[9]Department of OMNI Bioinformatics, Genentech, Inc., 1 DNA Way, South San Francisco, CA 94080, USA.

[10]Department of Molecular Biology, Genentech, Inc., 1 DNA Way, South San Francisco, CA 94080, USA.

[11]Department of Medicine, University of California, San Francisco, CA 94143, USA.

[12]Department of Biomarker Discovery OMNI, Genentech, Inc., 1 DNA Way, South San Francisco, CA 94080, USA.

*Correspondence: sun.tianhe@gene.com (T.S); arron.joseph@gene.com (J.R.A.).

SUPPLEMENTARY MATERIALS:

Materials and Methods

Fig. S1. Alignment of human TGFβ isoform sequences.

Fig. S2. Characterization of FL-TGFβ1, FL-TGFβ2 and FL-TGFβ3.

Fig. S3. Cellular composition and TGFβ3 expression in IPF lung samples.

Fig. S4. TGFβ2 and TGFβ3 expression in bleomycin-challenged mouse lung.

Fig. S5. Schematics of TGFβ2 and TGFβ3 conditional knockout.

Fig. S6. 6F12 and 4A11 inhibit mouse and human TGFβ2 comparably.

Fig. S7. Surface plasmon resonance sensorgrams for binding of the TGFβR2 to TGFβ ligands in the presence of anti-TGFβ antibodies.

Fig. S8. 4A11 binds to a different epitope of TGFβ2 than the TGFβR complex.

Fig. S9. TGFβ2 and TGFβ3 inhibition does not lead to enhanced immune responses that are associated with pan anti-TGFβ antibody treatment.

Table S1. Characteristics of isoform-selective anti-TGFβ monoclonal antibodies.

Table S2. Characteristics of humanized 4A11 clone.

Table S3. Data collection and refinement statistics for TGFβ2/4A11 structures.

Table S4. Amino acids in the 4A11 epitope interacting with TGFβ2 dimers.

Table S5. Primary amino acid sequences at various positions among TGFβ1, β2, β3 that interact with the 4A11 epitope.

Table S6. Anti-TGFβ isoform-specific antibodies all exhibited favorable pharmacokinetics in C57BL/6 mice.

Data file S1. raw data.

MATERIALS AND METHODS

Animals

Mice

All animal experiments were approved by the Institutional Animal Care and Use Committee at Genentech, Inc. C57BL/6 mice were obtained from Jackson Laboratories or Envigo. *SPC- CreER^{T2}; Rosa-LSL-tdTomato (SPC-WT-Tm)* mice were provided by Dr. Brigid Hogan and bred in house (*15, 16*).

Generation of TGFβ2 and TGFβ3 conditional knock-out (cKO) mice

Tgfb2$^{fl/fl}$ and *Tgfb3$^{fl/fl}$* mice were generated at Genentech. Exons 6 of both *Tgfb2* and *Tgfb3* genes encode the majority of sequence in the mature forms of TGFβ proteins, and were therefore previously targeted in TGFβ2 and TGFβ3 germline knockout mice (*8-10*). We introduced two loxP sites flanking exons 6 in *Tgfb2* and *Tgfb3* alleles to create *Tgfb2$^{fl/fl}$* and *Tgfb3$^{fl/fl}$* mice, respectively (Fig. S5). To generate *Tgfb2$^{fl/fl}$* or *Tgfb3$^{fl/fl}$* embryonic stem (ES) cell clones, C57BL/6N C2 ES cells were electroporated with linearized targeting vector DNA and cultured under drug selection. Positive clones were identified using long range PCR followed by sequence confirmation. Correctly targeted ES cells were subjected to karyotyping. Euploid gene-targeted ES cell clones were treated with Adeno-FLP to remove PGK neomycin and ES cell clones were tested to identify clones with no copies of the PGK neomycin cassette and the correct sequence of the targeted allele was verified. The presence of the Y chromosome was verified before microinjection into albino Bl/6N embryos. Germline transmission was obtained after crossing resulting chimeras with C57BL/6N females. Genomic DNA from pups was screened by long range PCR to verify the desired gene targeted structure before mouse colony expansion.

Genotyping primers in *Tgfb2* allele:

TGFb2cko_1 (5' loxP): CCATAGAGGCAGGAATGT

TGFb2cko_2 (inside loxPs): AGCACAGAAGTTAGCATTG

TGFb2cko_3 (3' loxP): AACACAAGCAAGAGGATTG

Expected PCR products sizes in various alleles:

Primers 1 and 2: WT (435bp); floxed (469bp)

Primers 1 and 3: KO (303bp)

Genotyping primers in *Tgfb3* allele

TGFb3-1 (5'loxP): CCTGGAATGGGAGAAGTCAA

TGFb3-2 (inside loxPs): ACAACGTTCTGATCTTGGCAG

TGFb3-3 (3'loxP): AGTGACATGCGACAGCTGAA

Expected PCR products sizes in various alleles:

Primers 2 and 3: WT (265bp); floxed (351bp)

Primers 1 and 3: KO (562bp)

Conditional double knockout (cDKO) mice were generated by breeding together these two cKO alleles. cKO or cDKO strains were then bred to the *ROSA26-CreER^{T2}* mouse strain (*67*). Induction of *CreER^{T2}* alleles was done by i.p. injection of 80mg/kg tamoxifen (Cat# T5648; Sigma) in sunflower oil (S5007-1L; Sigma) for five consecutive days. Subsequent studies were initiated at least one week after the completion of tamoxifen treatment. For antibody administration, mice were treated intraperitoneally with anti-TGFβ or control antibodies in saline at indicated concentrations and frequencies, between day 0 and days 14 or 24 for bleomycin studies, between day 0 and day 42 for CCl_4 studies, and between day 0 and day 24 for the colitis study.

Lung genomic DNA isolation and Quantitative PCR

Genomic DNA was isolated from mouse whole lungs using the DNeasy Blood & Tissue Kit (Cat# 69506; Qiagen). TGFβ DNA quantities were examined by qPCR using Taqman

Copy Number Assays (Applied Biosystems). Threshold cycle values (Ct) were normalized to an internal reference, *Tert* (ΔCT). The genomic DNA quantities were calculated by the $2^{-\Delta\Delta CT}$ method. The following Taqman assays from Applied Biosystems were used:

Tgfb2 Exon3 (Mm00035180_cn)

Tgfb2 Exon6 (Mm00035822_cn)

Tgfb3 Exon3 (Mm00381025_cn)

Tgfb3 Exon6 (Mm00381036_cn)

and *Tert* (4458373).

Rabbits

New Zealand White (NZW) rabbits purchased from Western Oregon Rabbit Company (WORC) were immunized at a local contract research organization following the guidelines for animal care under the regulation of Roche Institutional Animal Care and User Committee (Roche IACUC) and Genentech Laboratory Animal Resources (LAR) requirements.

Rats

Sprague Dawley rats were purchased from Charles River (Hollister, CA) and were immunized following the guidelines for animal care under the regulation of Roche Institutional Animal Care and User Committee (Roche IACUC) and Genentech Laboratory Animal Resources (LAR) requirements.

Mouse Lung Alveolar Organoid Culture and Secretome Library Screening

Lung cell isolation and AEC2 cell sorting

Lung cells were isolated following a previously published protocol (*77*). Tissues were disrupted and single cells were collected after lungs were inflated and digested with a

protease solution cocktail (5U/ml Dispase, 450U/ml Collagenase Type I, 4U/ml Elastase and 0.33U/ml DNaseI in DMEM/F12) for 45 minutes at 37^{o}C with frequent agitation. Cells were then washed with DMEM with 10% Fetal Bovine Serum (FBS, Invitrogen) and resuspended in ACK lysis buffer for 3 minutes to lyse red blood cells. After washing, cells were blocked by purified rat anti-mouse CD16/CD32 antibody (Cat# 553142; BD Biosciences) and stained with antibodies for CD45 (Cat# 17-0451-82, eBioscience), EpCAM (Cat#11-5791-82, eBioscience). AEC2 cells were sorted on a BD FACSAria Fusion cell sorter (BD Biosciences), based on the following markers: CD45^{-}; EpCAM^{+}; and tdTomato^{+}. Data were analyzed with Flowjo software.

Alveolar epithelial cell (AEC) 3-D organoid culture

AEC organoid culture was performed according to a previously published protocol with minor modifications (*15, 16*). Sorted AEC2 cells were mixed with human stromal cell NHLF (Cat# CC-2512; Lonza Walkersville Inc. USA) at a 1:10 ratio. The cells were resuspended in pre-chilled 1:1 mixed media of MTEC/Plus and growth factor–reduced Matrigel (Cat# 356231; BD Biosciences). 10^4 AEC2 cells and 10^5 NHLF cells were placed in 90µl mixed media in a 24-well 0.4-µm transwell insert (Cat# 3470; Costar). 500µl MTEC/Plus media was added to the lower chamber. Media were changed every other day. Organoids were assessed after 12-14 days of culture by inverted fluorescence microscope.

Microscopy

Whole organoid culture images were captured on a Nikon Ti-E Perfect Focus inverted microscope. Large images were generated by automatically stitching multiple adjacent frames from a multipoint acquisition using a motorized stage. Images were analyzed by ImageJ software.

Secretome Library Screening

The Secretome library was generated at Genentech Inc. to support in-house functional screening. It comprises a collection of plasmids expressing individual human cDNAs in mammalian expression vectors, with ~1,700 individual full-length genes that encode secreted proteins. To identify factors that may be involved in AEC biology in the alveolar organoid system, we first divided the library into 96 sub-libraries, each containing around 10-20 individual plasmids. We transiently transfected each sub-library plasmid pool into 293T cells using Lipofectamine 2000 (Cat# 11668019, ThermoFisher) according to the manufacturer's recommendations. Conditioned media were collected two days later and kept at $4^{O}C$ until being added to alveolosphere cultures. Positive sub-libraries were identified at the end of the culture. During the second round of screening, conditioned media from individual plasmids in each positive sub-library were generated and tested.

Biochemical Characterization of TGFβ Activity

Protein Expression Constructs

The cDNAs of human full-length *TGFB1*, *TGFB2*, *TGFB3*, and integrins αv (*ITGAV*) and β6 (*ITGB6*) genes were cloned into the mammalian expression vector, pRK5 (*78*). To generate RGE mutations in TGFβ1 and β3, aspartic acid (D) was substituted by glutamic acid (E) at the RGD domains in human full-length TGFβ1 (position 217) and TGFβ3 (position 240). To generate mutations at furin cleavage sites, the RXR/KR domain in the human TGFβ were substituted by RHAA, AHRR (for TGFB1) or RKAA (for TGFB2 and TGFB3), respectively.

Transfection and Co-culture

Human 293T cells were transfected with expression plasmids as indicated. Two days later, 10^4 transfected cells were co-incubated with $2X10^4$ MLEC reporter cells in 75μl assay media (DMEM high glucose with 0.5% heat inactivated FBS, 2 mM L-glutamine

and 0.5% Penicillin Streptomycin) in a 96-well plate. The luciferase activity was determined as described below. Cytochalasin D (Cat# C2618, Sigma) was added at 10μM at the beginning of the co-culture when indicated. For supernatant collection, cell media were replaced by DMEM containing 0.5% FBS the day after transfection. Supernatants were collected 24 hours thereafter and TGFβ activity was measured by reporter assays. To assess total TGFβ activity, supernatants were acidified by adding 1/5 volume of 1N HCl, incubated at room temperature for 10 minutes, and neutralized with 1/5 volume of 1.2N NaOH/0.5M HEPES (*68, 69*). Simian COS-7 cells (CRL-1651, ATCC) were used as another transfection recipient where indicated.

Generation of recombinant fusion proteins

To generate human Fc-fusion proteins, Fc regions (CH2 and CH3 domains) of the human IgG1 heavy chain and the hinge region was fused to the N-terminus of full-length TGFβ proteins or LAP domains to give rise to Fc-FL-TGFβ1, Fc-FL-TGFβ2, Fc-FL-TGFβ3, Fc-LAP1, Fc-LAP2, and Fc-LAP3 respectively. To support future in vivo studies, an RGE mutation was introduced in the RGD region in the Fc-LAP1 fusion protein. To increase protein expression and avoid inappropriate disulfide bond formation (*79*), all fusion proteins carried the C4S mutation at the start of their latency associated peptides.

TGFβ activity assay

TGFβ activity was measured using mink lung cells (MLEC) transfected with a plasmid containing the luciferase gene downstream of the plasminogen activator inhibitor 1 promoter as described (*19*). Anti-TGFβ antibodies or Fc fusion proteins were incubated with each TGFβ isoforms (Cat# 100-21; 100-35B; 100-36E, PeproTech, Rocky Hill, NJ and Cat#7346-B2, RnD systems) at 25°C for 1 h prior to the addition into 4 x 10^4 MLE reporter cells seeded in 96-well plates in 75 μL of assay buffer. Plates were incubated at 37°C and 5% CO_2 for 20 hours. Luciferase activity in cells was determined

by adding Firefly Luciferase substrate according to the manufacturer's recommendations (Cat# E1910, Dual-Luciferase Reporter Assay System, Promega). Alternatively, a transfected human HEK293 cell based (HEK-Blue™ TGF-β) cell line (Cat# hkb-tgfb, InvivoGen) was used as the reporter instead, following manufacturer's recommendations. The SEAP concentrations in the supernatants were determined by QUANTI-Blue™assay according to the manufacturer's instructions (Cat# rep-qbs, InvivoGen). 19D8 (Cat #521707, Biolegend) was used as the anti-TGFβ1 antibody in the assay.

Western assay

Human stromal NHLF cells (Cat# CC-2512; Lonza Walkersville Inc. USA) were seeded at $2x10^6$/100-mm culture dish overnight. Cells were serum starved in DMEM with 0.5% FBS for 24 hours, before treatment with supernatants (1:7 diluted in PBS), recombinant TGFβ1 (3ng/ml), or recombinant BMP2 (200ng/ml) as indicated. At specified times, cells were immediately washed with ice cold PBS buffer and lysed in ice cold lysis buffer (RIPA buffer with protease inhibitor cocktail (Cat# 4693159001, Roche) and phosphatase inhibitor cocktails 2 and 3 (Cat# P5726 and P 0044, Sigma)). Protein concentration in each cell lysis was quantified by Pierce™ BCA Protein Assay Kit (Cat #23225, ThrmoFisher). Western blot analysis was performed by loading exactly 20μg protein per lane in 4-20% Tris-Glycine SDS-PAGE Gels (Cat# XP04200BOX, ThermoFisher) followed by transfer to nitrocellulose membranes (Cat# LC2001, ThermoFisher). The blots were probed by anti-pSmad2 antibody (Cat#3108; cell signaling), and detected by a HRP-conjugated secondary antibody (Cat#111-035-144, Jackson ImmunoResearch) and Amersham ECL detection reagents (RPN2109, GE Healthcare).

To detect the Furin site mutated TGFβ proteins, supernatants were run in SDS-PAGE in reducing conditions. TGFβ1 and TGFβ2/3 proteins were detected by two different rabbit polyclonal antibodies: anti-TGFβ1 (Cat#3711, Cell Signaling;) and anti-TGFβ2/3 (Cat#ab15537, Abcam).

Gene Expression Analysis

Single-cell RNA sequencing sample processing, library preparation and analysis

Preparation of human lung tissue:

Explanted lung tissues were obtained from patients with a pathologic diagnosis of usual interstitial pneumonia and a consensus clinical diagnosis of IPF assigned by multidisciplinary discussion and review of clinical materials. Written informed consent was obtained from all subjects and the study was approved by the UCSF institutional review board. After bronchoalveolar lavage, fresh lung explant tissue was stored in complete media on wet ice overnight. The tissue was washed in HBSS and then thoroughly minced in digestion buffer (HBSS, 2.5mg/mL Collagenase D, 100 μg/mL DNase I). Minced tissue was rocked 45 minutes at 37°C. Residual tissue material was transferred into fresh digestion buffer and rocked another 45 minutes at 37°C. Single cells from both rounds of digest were combined and utilized for downstream analyses. Remaining tissue was processed using a gentleMACS Dissociator (Miltenyi Biotec) to liberate additional cells into a single cell suspension. This preparation was then filtered and added to the previously isolated cells.

FACS Isolation of cell populations:

Total number of cells were determined and resuspended in appropriate volume of 1x PBS supplemented with 2mM EDTA and 2% fetal bovine serum (FBS). FcR blocking was performed using the Miltenyi Biotec FcR blocking reagent according to manufacturer's protocol. Cells were then stained with a cocktail of antibodies including CD45-BUV395 (Cat#563792; BD biosciences), EPCAM-PE (Cat # 566841, BD), CD31-BV605 (Cat #562855, BD), and Live/Dead-Efluor 780 (Cat # 65-0865-14, BD) on ice for 30 minutes and then washed with supplemented PBS buffer 3 times. 5 populations of cells were collected for downstream library preparation: Unsorted live cells, $CD45^{+}$, $CD45^{-}$

/EPCAM^{+}, CD45^{-}/CD31^{+}, and CD45^{-}/CD31^{-}/EPCAM^{-}(triple negative).

Library preparation and sequencing:

Single-cell library preparation was performed on the 10x Genomics platform using Chromium Single Cell 3' Library and Gel bead kit v2 following manufacturer's user guide (10x Genomics). Cell density was used to impute the volume of single cell suspension needed in the reverse transcription (RT) master mix, aiming to achieve ~6,000 cells per sample. cDNAs and libraries were prepared following manufacturer's user guide (10x Genomics). Libraries were profiled by Bioanalyzer High Sensitivity DNA kit (Agilent Technologies) and quantified using Kapa Library Quantification Kit (Kapa Biosystems). Each library was sequenced in one lane of HiSeq4000 (Illumina) following the manufacturer's specifications (10x Genomics).

Processing and analysis of sequencing data:

Sequencing reads were assembled and aligned against the GRCh38 human reference using Cell Ranger v3.0.2 (10x Genomics, Pleasanton, CA, USA). Expression count matrices were analyzed using the Seurat v3.1 (*80*) R package (*81*). Only cells with ≥ 500 features and ≤ 25% total mitochondrial feature counts where retained for analysis. Normalization was performed using the log-normalization method. Approximately 4000 highly-variable features were selecting using the mean/variance regression method for sample integration and clustering after removal of immunoglobulin and T cell receptor variable domain features from the highly-variable feature set. Sample integration and batch correction was performed using anchor-based sample integration (*80*). Clustering was performing using 30 PCA components on a k=20 shared nearest neighbor (SNN) graph using the Louvain algorithm. t-SNE dimensional reductions were performed using Rtsne v0.15 (*82*). Marker selection was performed using the Wilcoxon Rank Sum test on the integrated sample data for each cluster against all clusters. Cell type

annotations were performed manually based differentially expressed markers meeting the criteria of: an average log fold-change compared to all other clusters of at least 0.8; being either detected (detection defined as having ≥ 1 UMI for the feature) in ≥ 50% of the cells in a given cluster or detected in ≤ 10% of all other clusters; and showing no clear evidence of ambient RNA contamination. Single cell RNA-seq data from human IPF lung was deposited in the NCBI Gene Expression Omnibus (GEO) database under accession GSE159354.

Microarray Analysis

Gene expression kinetics from whole lung after IT bleomycin instillation were determined from a published dataset (*27*); Gene Expression Omnibus (GEO) accession GSE37635. Gene expression in human normal vs. IPF lung samples was determined from a published dataset (*25*); GEO accession No. GSE53845. Gene expression in human NASH patient liver samples was determined from a published dataset (*34, 35*); GEO accession NO. GSE49541.

RNA sequencing

Mouse whole lungs were harvested at day 14 after bleomycin administration, N=5 in the saline control group, N=8 in the bleomycin group. Single cells were isolated after protease digestion following our previously published protocol (*16*). After washing, cells were blocked by purified rat anti-mouse CD16/CD32 antibody (Cat# 553142; BD Biosciences) and stained with antibodies for CD45 (Cat# 17-0451-82, eBioscience), EpCAM (Cat#11-5791-82, eBioscience), and CD31 (Cat#25-0311-82, eBioscience). Four cell populations from each mouse were sorted based on their cell surface markers: leukocytes ($CD45^+$; $EpCAM^-$); epithelial cells ($CD45^-$, $EpCAM^+$); endothelial cells ($CD45^-$; $EpCAM^-$; $CD31^+$); and fibroblasts (triple negatives). RNA was purified from the sorted cells using the RNeasy Mini Kit (Cat#74106; Qiagen). 0.5 µg of total RNA was

used as an input material for library preparation using TruSeq RNA Sample Preparation Kit v2 (Illumina, San Diego CA), which was quality controlled with Fragment Analyzer and a Library quantification kit (KAPA Biosystems, Wilmington MA). Libraries were multiplexed and then sequenced on Illumina HiSeq2500 to generate 30M single end 50 base pair reads. Sequencing reads were mapped to the reference mouse genome (GRCm38), using the GSNAP short read aligner (Wu and Nacu, 2010), and assigned to RefSeq gene models. Expression was measured in normalized reads per kilobase per million total reads (nRPKM). RNAseq data on sorted cell populations in the bleomycin model were deposited in the NCBI Gene Expression Omnibus (GEO) database under accession GSE168529.

Animal Models

Bleomycin administration, deuterated water labeling, and hydroxyproline measurement

Adult mice (>12 weeks) were randomized based on pre-study weights to minimize variance between experimental and control groups. For intratracheal (IT) dosing, all mice were lightly anesthetized with isoflurane in an induction chamber. Once anesthetized, the animals were removed from the chamber, manually restrained, the mouth of the animal was opened and the tongue set aside. A 1 ml syringe with 50 microliters of sterile injectable isotonic saline or bleomycin (0.70U/kg (DNC# 0703-3155-01; TEVA) in 50 μl sterile isotonic saline) was connected to a 24 gauge gavage needle. The gavage needle was inserted into the trachea and a dose of either vehicle or bleomycin was delivered intratracheally. After delivery, animals were monitored continuously until fully awake and ambulatory.

Deuterated water labeling was used previously to assess the new collagen synthesis in bleomycin studies (*16, 27, 70*). In our studies, the labeling was started on the 9th day

after bleomycin delivery, by i.p. injecting deuterated water (Cat# DLM-4-99.8-1000; Cambridge Isotope Laboratories) 35 ml/kg in 2 divided doses 4 hours apart. Afterward, 8% deuterated water in drinking water was provided ad lib in a water bottle until the end of the study.

Deuterated water incorporation into hydroxyproline was analyzed as described previously (*16, 71*). Mass spectrometry and analysis were performed by Metabolic Solutions. New hydroxyproline content was expressed as "μg per lung."

CCl_4 model

8-10 week-old male C57BL/6J mice (Jackson West) were IP injected with 0.5ml/kg body weight carbon tetrachloride (Sigma-Aldrich,#319961, 1:6 v/v diluted in corn oil) or corn oil (Sigma-Aldrich) three times per week for 6 weeks. Mice received anti-TGFβ2/3 (4A11)-mIgG2a-LALAPG antibody or control (anti-gp120-mIgG2a-DANA) three times per week at 10 mg/kg for 6 weeks. The animals were sacrificed 72 hours after the final CCl_4 injection and whole livers and serum were collected for histological and molecular analysis.

Colitis model

8-10-week-old C57BL/6 mice (Envigo) were inoculated orally with 0.2ml $1X10^9$ cfu/ml *Helicobacter Hepaticus* suspension for two consecutive days. Mice were treated with anti-IL10R antibody (Cat# BE0050, BioXCell) weekly at 1mg/mouse to induce colitis. To test the effects of anti-TGFβ antibodies, mice were received pan anti-TGFβ (1D11), anti-TGFβ2/3 (4A11), or control antibody three times per week at 10 mg/kg until the end of the study. The animals were euthanized at day 24, and mouse intestines were isolated, weighed and proceeded as indicated.

Mouse intestine lamina propria were isolated from cecums and proximal colons according to the manufacturer's recommendation (Cat #130-097-410, Miltenyi). Total cell numbers were determined and cells were stained with antibodies for CD3e (Cat# 553064, BD Biosciences), CD4 (Cat#553729, BD Biosciences), CD8 (Cat#553036, BD Biosciences), CD11b (Cat#553312, BD Biosciences,), Ly6G (Cat#551460, BD Biosciences), Ly6C (Cat#1760-09, Southern Biotech) . Data was analyzed by Flowjo software.

RNA isolation and Quantitative RT-PCR from mouse tissues

Whole mouse lungs (bleomycin studies), mouse proximal colons (colitis study) or mouse liver lobes (CCl_4 studies) were isolated. Tissues were processed using a gentleMACS Dissociator (Miltenyi Biotec) for tissue homogenization. RNA was extracted from the tissue homogenates using RNeasy Mini Kit (Cat#74106; Qiagen). Gene expression were quantified by RT-qPCR using Taqman RNA-to-C_T 1-Step Kit (Cat# 4392938; Applied Biosystems). The reactions were run on a QuantStudio 6 Flex Real-Time PCR System (ThermoFisher). Threshold cycle values (Ct) were normalized to a housekeeping gene, GAPDH (ΔCT). Relative gene expression was calculated by the $2^{-\Delta\Delta CT}$ method.

The following Taqman gene expression assay kits from Applied Biosystems were used:

Serpine1 (Mm00435858_m1)

Fn1(Mm01256744_m1)

Col1a1 (Mm00801666_g1)

Col3a1 (Mm01254476_m1)

Tgfb1 (Mm01178820_m1)

Tgfb2 (Mm00436955_m1)

Tgfb3 (Mm00436960_m1)

Il6 (Mm00446190_m1)

Tnf (Mm00443258_m1)

Ifng (Mm01168134_m1)

Gapdh mouse (Cat#4352661)

Immunohistochemistry, Histology and Pathology Analysis

Immunohistochemistry for pSMAD3 and in situ hybridization for TGFβ3 in human IPF

Immunohistochemistry for phoshpho-SMAD3 was performed on formalin-fixed, paraffin-embedded sections using a rabbit monoclonal antibody (EP823Y, 0.76 µg/ml; Abcam). Briefly, sections were depariffinized and used for immunhistochemistry on an automated staining platform (Bond RX; Leica Biosystems) using proprietary reagents for antigen retrieval (ER2; Leica Biosystems) and detection of bound primary antibody (anti-rabbit PowerVision polymer-HR; Leica Biosystems). Signal was visualized using DAB. Combined dual ISH/IHC was performed on formalin fixed paraffin embedded tissue using a commercially available probe set for human *TGFB3* (ACD Cat # 464478; nt2022-3020) and a primary antibody against pSMAD3 (Abcam, EP823Y). Briefly, sections were deparaffinized and used for ISH using standard conditions according to the probe manufacturer (ACD RNAscope 2.5 LSx kit) on an automated staining platform (Leica Bond III). Slides were then subjected to the IHC sequence using the same staining platform. Primary antibody at 1.5 µg/ml was incubated for 60 min at ambient temperature. Detection was performed using the PowerVision HRP kit (Leica) in combination with a green chromogen (Nordic Biosite, BCB-BMWWP9-1) for visualization.

Histological analysis of mouse lung fibrosis in the bleomycin induced model

Formalin fixed samples of mouse lungs (5 lobes) were embedded as a whole and processed to 1 slide per animal, stained with H&E or Masson's Trichrome. Alternatively, fibrosis was evaluated by immunohistochemistry using anti-collagen III antibody (Cat#ab7778, Abcam). The extent of pulmonary fibrosis was scored according to the following criteria:

(A) Interstitial fibrosis pattern – number of foci: 0, none detected; 1, ≤ 10; 2, ≤ 15; 3, >

15/ all sections, but distinct; 4, multifocally coalescent or locally extensive; 5, diffused

(B) Interstitial fibrosis -- size of foci: 0, none detected; 1, largest focus ≤ area of ~ 2 alveolar spaces; 2, largest focus ≤ area of ~ 4 alveolar spaces; 3, coalescent (> 4 patent alveolar spaces); 4, locally extensive (60-90 % of an entire lobe); 5, diffuse (> 90% of an entire lobe);

(C) Total scores: number of foci x size of foci

Histological analysis of mouse liver fibrosis in the CCl_4 model

Formalin fixed samples of mouse livers were processed. For each animal, one section was stained with H&E and one section was stained with Trichorme. Lesions are scored blinded to group identities for degrees of architectural disruption and extent of fibrosis based on a previously published method (*83*).

Generation and Characterization of Isoform Specific Antibodies

Generation of rabbit anti-human TGFβ monoclonal antibodies

New Zealand white rabbits were immunized with human TGFβ2 and TGFβ3 isoforms (Peprotech) and single B-cells were isolated using a modified protocol related to published literature (*84*). Briefly, rabbit peripheral blood mononuclear cells (PBMCs) were isolated for IgG B cell enrichment by immunofluorescence staining with biotinylated anti-rabbit CD11b antibody, anti-rabbit T-lymphocyte antibody (AbD Serotec, BioRad) and anti-rabbit IgM (BD Bioscience) to further deplete rabbit myeloid cells, T cells and IgM B cells through MACS Column (Miltenyl Biotec) according to the manufacturer's instructions. The following workflow included using FITC-labeled goat anti-rabbit IgG antibody (Serotec, BioRad), APC-labeled human TGFβ1 (Innova Biosciences) and RPE-labeled human TGFβ2/3 (Innova Biosciences) to sort rabbit IgG+ and human TGFβ2/3+-reactive single B cells into 96-well plate with culture medium and feeder cells for 7 days cultivation. The B-cell culture supernatants were subject to

primary ELISA screening for human TGFβ2/3 isoform binding, and B cells were lysed in RLT buffer and stored at -80°C. In the molecular cloning, the light chain and heavy chain variable regions of human TGFβ2/3 specific B cells were amplified by PCR and cloned into expression vectors as described (*84*). Each recombinant rabbit monoclonal antibody was expressed in Expi293 cells (Thermo Fisher Scientific, Waltham, MA) and subsequently purified with protein A. Purified anti-human TGFβ2/3 antibodies were then subjected to functional characterization in blocking, affinity determination.

Development of rat anti-human TGFβ hybridoma antibodies

Sprague Dawley rats (Charles River, Hollister, CA) were immunized with human TGFβ2 or TGFβ3 with Complete Freund's adjuvant or a Toll-like receptor cocktail adjuvant (MPL, Poly (I:C), R848, and CpG (Sigma-Aldrich, St. Louis, MO)). After biweekly boosts for 8 weeks, hybridomas were generated as described previously (*85*). Supernatants were screened by ELISA against human TGFβ ligands. Hybridomas demonstrating binding to human TGFβ2 or TGFβ3 by ELISA were scaled-up and supernatants were harvested and purified by protein G (GammaBind Plus, GE Healthcare, Pittsburgh, PA) for functional tests. Antagonist antibodies were submitted for sequencing and cloned out for recombinant production.

ELISA Screening

An enzyme-linked immunosorbent assay (ELISA) was developed to screen the binding of candidate clones to TGFβ1, TGFβ2, and TGFβ3. First, each TGFβ isoform (Peprotech) was immobilized to the wells of Grenier Bio-One 384-well ELISA plates with coating buffer (50mM carbonate, pH 9.6, GNE Media Prep A3004) at 1 μg/ml; 50 μL/well for overnight incubation at 4°C. Then the coated ELISA plates were washed 3 times with ELISA diluent buffer 100 μl per well (PBS/0.5% Tween20, GNE Media Prep A0300). Next the ELISA plates were blocked with ELISA diluent buffer 100 μl/well for one hour.

After blocking, the buffer was discarded and samples and controls were added from 96-well plates to 384-well plates (50 µl/well). Then the ELISA plates were incubated for 30 minutes at room temperature with shaking. Next the plates were washed three times with wash buffer (PBS/0.05% TWEEN 20, 20X Stock Hyclone SH3A649-01) 100ul/well. Then diluted HRP conjugate (Peroxidase AffiniPure Goat Anti-Rat IgG (H+L) Jackson ImmunoResearch Laboratories, INC. 112-035-003 diluted 1:10000, 50 µl/well) was added to each well and the ELISA plates were incubated for 30 minutes at room temperature. After incubation, plates were washed 3 times with wash buffer (100 µl/well) and then substrate was added (BIOFX TMB Substrate TMBW-1000-01, 50ul/well). After 5 minutes incubation at room temperature for 5 minutes, stop solution (BIOFX Stop reagent LBSP-1000-01, 50 µl/well) was added. Finally, the plates were read at 659 nm for absorbance.

Surface Plasmon Resonance (SPR) assay

To determine if the antibodies interfere with TGFβ binding to TGFβR2, surface plasmon resonance (SPR) Biacore™-T200 instrument (GE Healthcare) was used. Series S sensor chip coupled with goat anti-human antibodies (BR100839, GE Healthcare) was applied to capture human Fc-fusion TGFβR2 (341-BR-050, R&D systems) to achieve approximately 100 response units (RU). The free form of TGFβ (5nM) or the premixed form of TGFβ (5nM) with tested antibody (1D11, 2A10, 4A11 or 6F12 in 10-fold excess) was injected in HBS-EP buffer (100 mM HEPES pH 7.4, 150 mM NaCl, 3 mM EDTA, 0.05% (v/v) Surfactant P20) with a flow rate of 50 µl/min at 25 °C to observe response. The binding response was recorded and analyzed by Biacore T200 evaluation software version 2.0.

Generation of mouse chimeric antibodies

1D11 (pan TGFβ antibody) was originally derived from mice (*86*). Fab regions of the

isoform specific anti-TGFβ antibodies were fused to the Fc region of mouse IgG2a with a LALA-PG mutation to remove the effector function for in vivo mouse studies (*28*).

Humanization of rabbit anti-TGFβ2/3 (4A11) dual specific antibody

To humanize the 4A11 antibody, the hypervariable regions and framework residues in the Vernier zone (*87*) of the light chain and heavy chain were grafted into a selection of the closest human IGKV and IGHV germline frameworks respectively (Table S2). The resulting DNA sequences were codon optimized for human expression and subcloned into mammalian expression vectors. The variable light chain was cloned into a pRK mammalian cell expression vector containing the human kappa constant domain, and the variable heavy chain was inserted into a pRK mammalian cell expression vector encoding the full-length human IgG1 constant domain with a N297A mutation in the heavy chain constant region to prevent N-glycosylation and improve the antibody production efficiency.

Anti-TGFβ isoform specific antibody pharmacokinetics in C57BL/6 mice

Naive female C57BL/6 mice, age 8 to 12 weeks, were received single doses of anti-TGFβ isoform antibodies at 1 mg/kg or 10 mg/kg by either IP or IV routes. Blood samples were collected via retro-orbital bleeds and the terminal blood sample was collected via cardiac stick from each animal in each dosing group at various timepoints up to 14 or 21 days post-dose with three mice per timepoint, and processed to collect serum. Serum samples were analyzed for test article concentrations by ELISA methods. Mouse anti-mouse IgG2a[a] (BD Biosciences, San Jose, CA, USA) was used as the capturing reagent and rat anti-mouse IgG2a (heavy chain) conjugated to horseradish peroxidase (HRP) (GeneTex, Irvine, CA, USA), was used as the detection reagent. The serum concentration versus time data were used to calculate PK parameters in mouse using noncompartmental analysis

(Phoenix™ WinNonlin®, Version 6.4.0.768; Certara; Princeton, NJ). Nominal sample collection times and nominal dosing solution concentrations were used in the data analysis.

Crystallization

The mature form of TGFβ2 was made in house (*88*). Briefly, FL-TGFβ2 was expressed with CHO Ti stable cell line. Protein was purified with Ni-NTA, then was acidified and dialyzed in 0.1 M Na Citrate, pH 3 and loaded onto 5 ml SP HP column. The fractions that contained the protein of interest from SP pool was then further purified with Vydac C4 RP-HPLC. The fraction containing mature TGFβ2 was dialyzed directly into 1 mM HCl pH3.

The Fab fragment (4A11) under control of the PhoA promoter was expressed in E. coli overnight at 30ºC. The cells were pelleted by centrifugation at 6000 rpm for 15 minutes and lysed by microfluidization in PBS supplemented with 25mM EDTA and 1mM PMSF. Cell debris was removed by centrifugation at 10,000 rpm for 1 hour at 4°C. The resulting supernatant was run through a Protein G column equilibrated in PBS, and eluted with 0.58% acetic acid. Protein fractions were further purified by ion exchange chromatography (SP-Sepharose) in 20 mM MES (pH 5.5) and eluted with a gradient from 0 to 250 mM NaCl. 4A11 Fab/TGFβ2 complexes were typically mixed at 1:1 molar ratio and further purified using a Superdex-200 column equilibrated in 25 mM Tris–HCl (pH 7.5) and 200 mM NaCl. For crystallization, the complex samples were concentrated to 10 mg/ml.

4A11 Fab/TGFβ2 crystals were obtained by vapor diffusion at 19°C by mixing equal volumes of protein plus 20% PEG 1000 and 01.m Tris pH8.5 well solution. Crystals were cryoprotected with 25% glycerol. Data set was collected at the Advanced Light Source beam lines 5.0.2 and processed with the HKL package (*89*).

Structure determination and analysis

Crystal structures were solved by molecular replacement using Phaser (*72*). The refined coordinates of the TGFβ2 structure PDB file (6I9J) (*73*) served as the search probe for the structure for TGFβ2. Subsequently, the Fc and Fv portions of the Fab were placed separately using Phaser and underwent initial rounds of rigid-body refinement with Phenix (*74*). The model went through several iterative rounds of adjustment with Coot (*75*). Atomic models were then built and refined with Refmac (*76*).

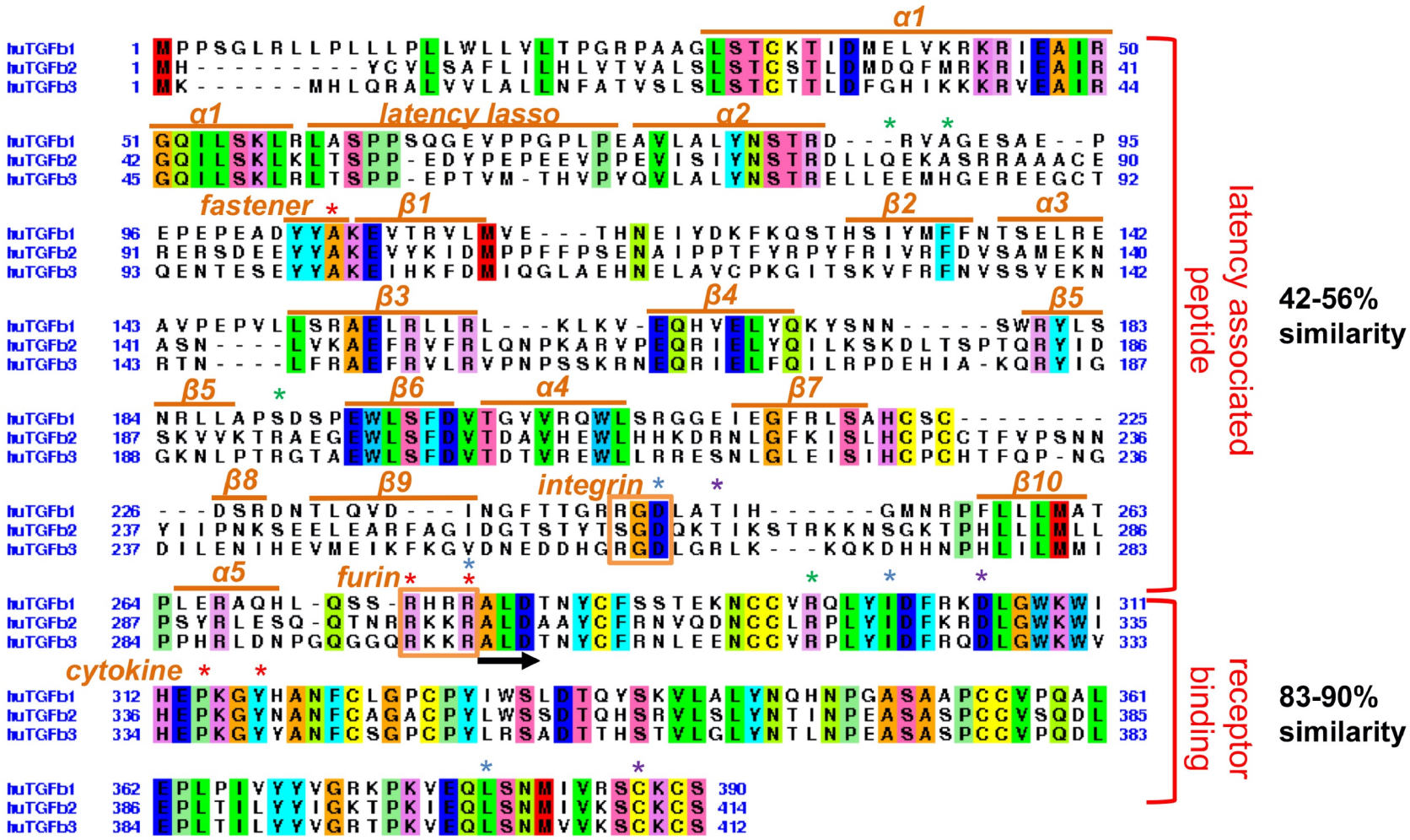
α1
α1
latency lasso
α2
fastener
β1
β2
α3
β3
β4
β5
β5
β6
α4
β7
β8
β9
integrin
β10
α5
furin
cytokine
latency associated peptide
receptor binding
42-56% similarity
83-90% similarity

Fig. S1. Alignment of human TGFβ isoform sequences. Primary sequence alignment of human TGFβ1, 2, and 3 with domains of TGFβ1 (α-sheets and β-strands, latency lasso, fastener, integrin-binding, furin cleavage, and cytokine) indicated as per Shi et al. (*51*). Residues are numbered from the predicted ATG (methionine) start site; Shi et al numbering starts from L30 at the start of the α1 helix. The black arrow underneath the sequences indicates the start of the receptor-binding domain. Loss-of-function point mutations in TGFβ2 and TGFβ3 described in Loeys-Dietz syndrome patients in (*52-54*) are indicated with red, blue, green, and purple asterisks, respectively. Frameshift, premature stop, and splice site mutations reported for TGFβ2 and TGFβ3 are omitted for clarity.

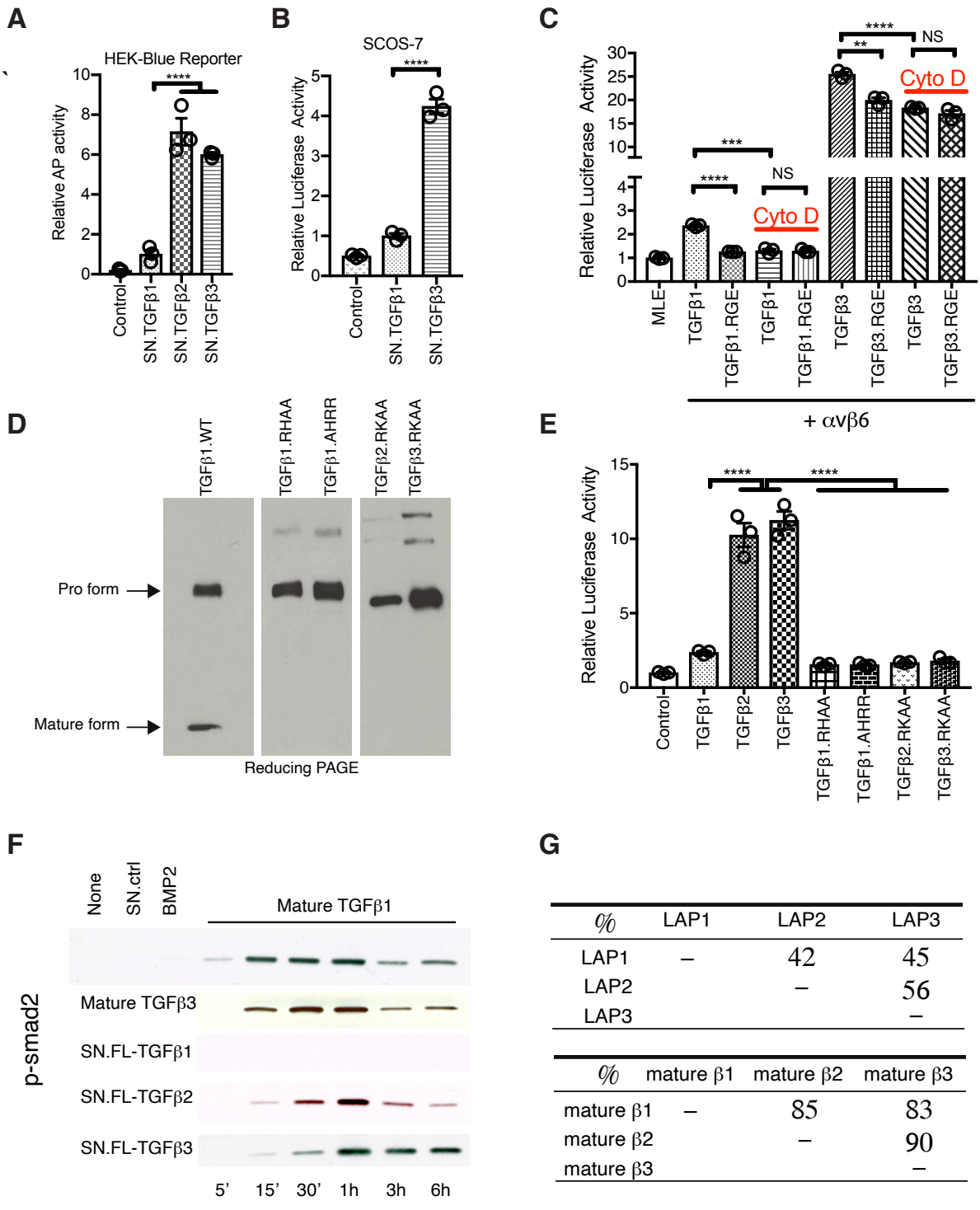

%	LAP1	LAP2	LAP3
LAP1	–	42	45
LAP2		–	56
LAP3			–

%	mature β1	mature β2	mature β3
mature β1	–	85	83
mature β2		–	90
mature β3			–

Fig. S2. Characterization of FL-TGFβ1, FL-TGFβ2 and FL-TGFβ3.

(**A**) Supernatants were collected from 293T cells transfected with a plasmid encoding FL-TGFβ1, FL-TGFβ2, FL-TGFβ3 or an empty vector (control). TGFβ activity was assessed

by alkaline phosphatase released by HEK-Blue TGFβ reporter cells. (**B**) Supernatants were collected from COS-7 cells transfected with a plasmid encoding FL-TGFβ1, FL-TGFβ3 or an empty vector (control). TGFβ activity was measured with MLEC reporter cells. (**C**) 293T cells were transfected with plasmids encoding various forms of FL-TGFβ and integrins αv and β6. TGFβ activities were measured with MLEC reporter cells after co-culture. Cytochalasin D (30μM) was added at the beginning of the co-culture where indicated. (**D** and **E**) Supernatants collected from 293T cells transfected with plasmids encoding wild-type or furin site mutant FL-TGFβ proteins were (D) analyzed in a reducing SDS-PAGE gel. Western blotting was performed with anti-TGFβ antibodies to show the lack of mature peptide release of mutated proteins due to their resistance to the furin proteolytic cleavage. (E) Supernatants were incubated with MLEC reporters to show the loss of TGFβ activities with the mutated proteins. (**F**) Western blot showing the kinetics of smad2 phosphorylation in NHLF cells treated with recombinant proteins or supernatants. As controls, NHLF cells were also treated with supernatant from non-transfected cells (SN.ctrl) or the recombinant BMP2 for 1 hour. To control the loadings among different samples, protein concentrations of supernatants were measured by BCA and 20μg protein was loaded in each lane. (**G**) Primary amino acid sequence similarities among human TGFβ isoforms. Latency associated peptides (LAPs) and mature domains (active) were compared separately.

(A-C and E) **, $P < 0.01$; ***, $P<0.001$; ****, $P < 10^{-4}$; NS, $P > 0.05$ by unpaired two-tailed Student's *t*-test. Data are averages ± SEM from experiments run in triplicate. Error bars are not shown when they are shorter than sizes of their corresponding symbols.

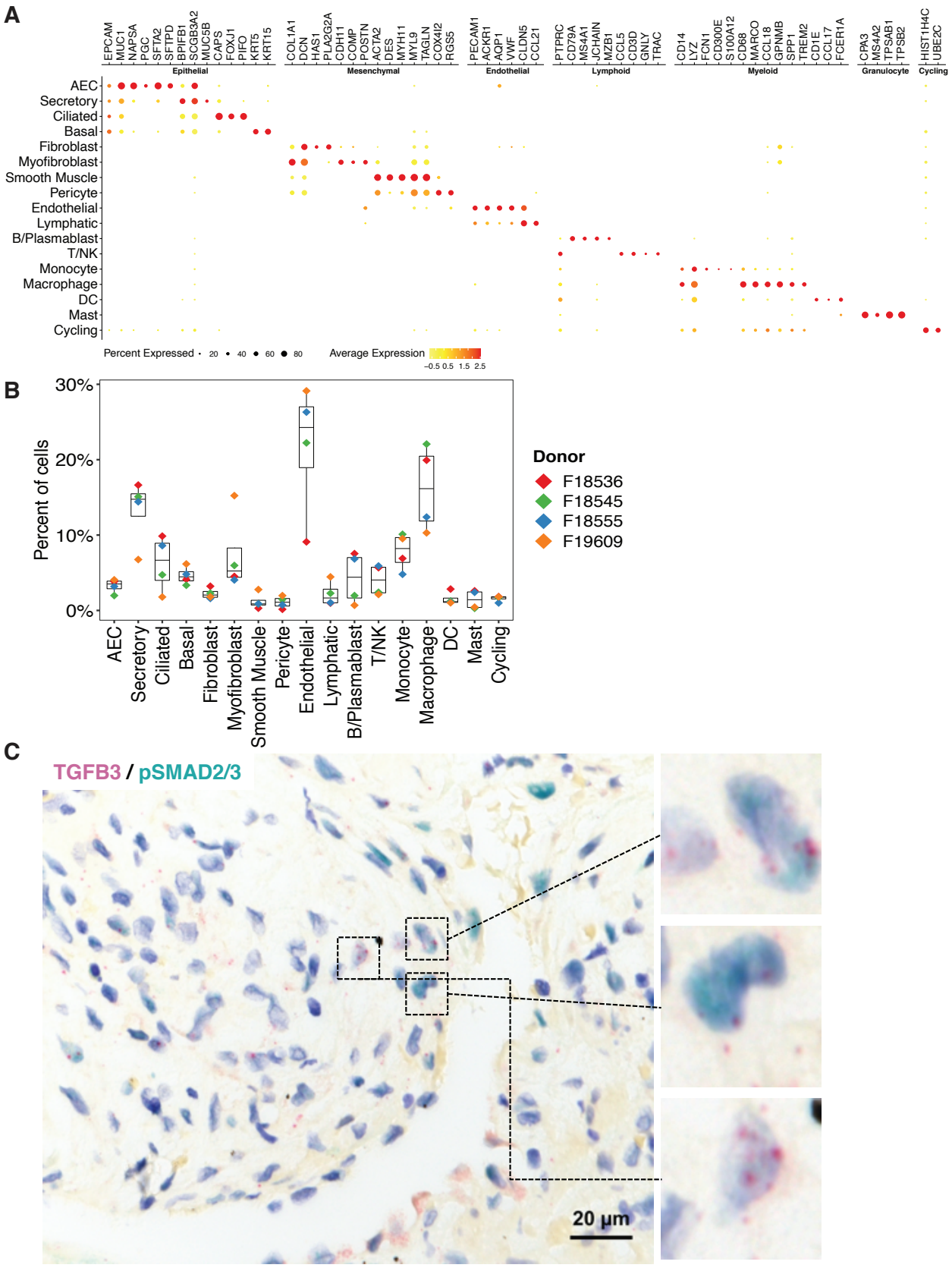
A
EPCAM
MUC1
NAPSA
PGC
SFTA2
SFTPD
BPIFB1
SCGB3A2
MUC5B
CAPS
FOXJ1
PIFO
KRT5
KRT15
COL1A1
DCN
HAS1
PLA2G2A
CDH11
COMP
POSTN
ACTA2
DES
MYH11
MYL9
TAGLN
COX4I2
RGS5
PECAM1
ACKR1
AQP1
VWF
CLDN5
CCL21
PTPRC
CD79A
MS4A1
JCHAIN
MZB1
CCL5
CD3D
GNLY
TRAC
CD14
LYZ
FCN1
CD300E
S100A12
CD68
MARCO
CCL18
GPNMB
SPP1
TREM2
CD1E
CCL17
FCER1A
CPA3
MS4A2
TPSAB1
TPSB2
HIST1H4C
UBE2C
Epithelial
Mesenchymal
Endothelial
Lymphoid
Myeloid
Granulocyte
Cycling
AEC
Secretory
Ciliated
Basal
Fibroblast
Myofibroblast
Smooth Muscle
Pericyte
Endothelial
Lymphatic
B/Plasmablast
T/NK
Monocyte
Macrophage
DC
Mast
Cycling
Percent Expressed 20 40 60 80
Average Expression
−0.5 0.5 1.5 2.5
B
Percent of cells
30%
20%
10%
0%
Donor
F18536
F18545
F18555
F19609
C
TGFB3 / pSMAD2/3
20 μm

Fig. S3. Cellular composition and TGFβ3 expression in IPF lung samples.

(A) Dot plot depicts exemplary transcripts for cluster assignment as depicted in Figure 3C. Cell identities were assigned on the basis of selected genes that distinguished individual clusters. Dot sizes correspond to proportion of cells in each cluster with detectable expression of indicated transcripts and colors correspond to expression intensity. **(B)** Distribution of cell type composition by subject (N=4 IPF donors). Primary data are available on GEO (accession number GSE159354). **(C)** Dual *TGFB3* in situ hybridization (magenta) and phospho-SMAD2/3 immunohistochemistry (teal) on a fibroblastic focus from IPF lung tissue (separate sample from Figure 3E).

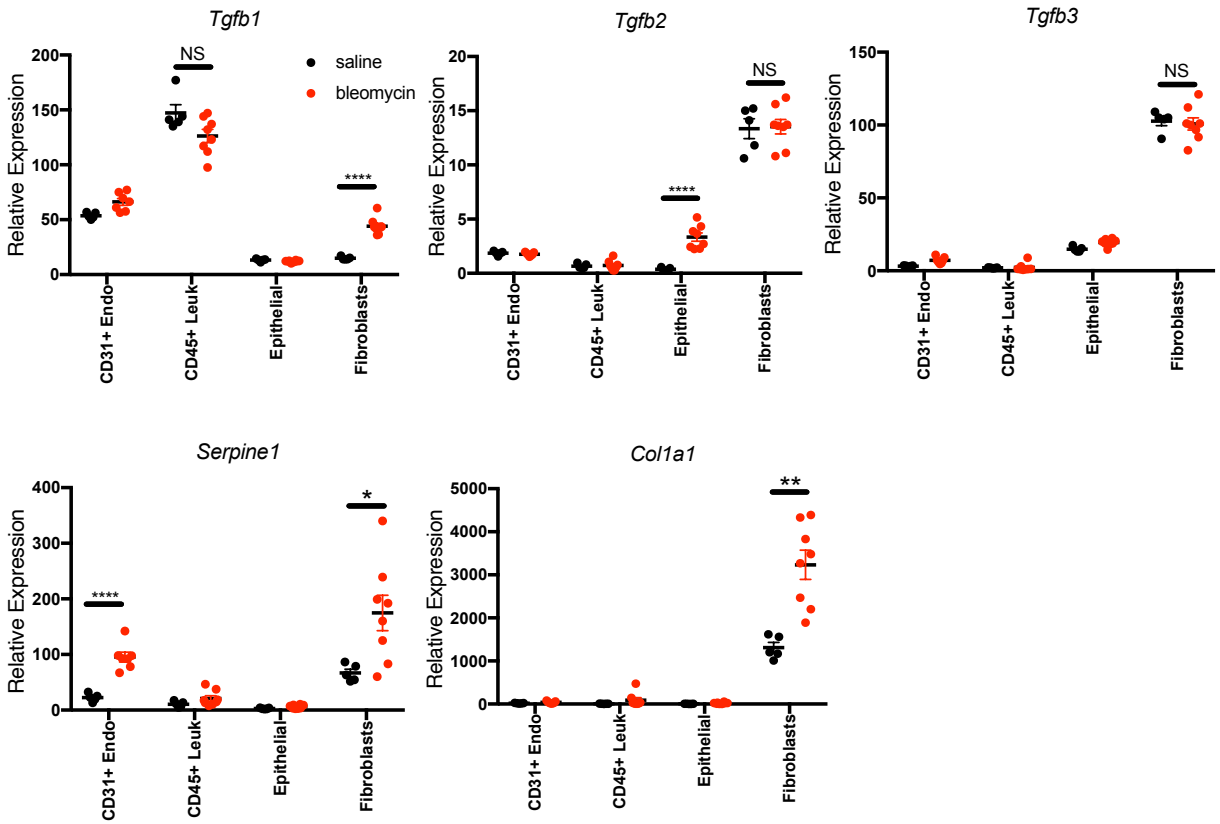

Fig. S4. TGFβ2 and TGFβ3 expression in bleomycin-challenged mouse lung.

Relative gene expression of TGFβ isoforms and TGFβ targeted genes, *Col1a1*, *Serpine1*, in multiple mouse lung cell types are shown. RNAseq was performed on sorted cell populations from the mice 14 days after treated with saline (n = 5) or bleomycin (n = 8). *, $P < 0.05$; **, $P < 0.01$; ****, $P < 10^{-4}$; NS, $P > 0.05$ by unpaired two-tailed Student's *t*-test. Data represent means ± SEM.

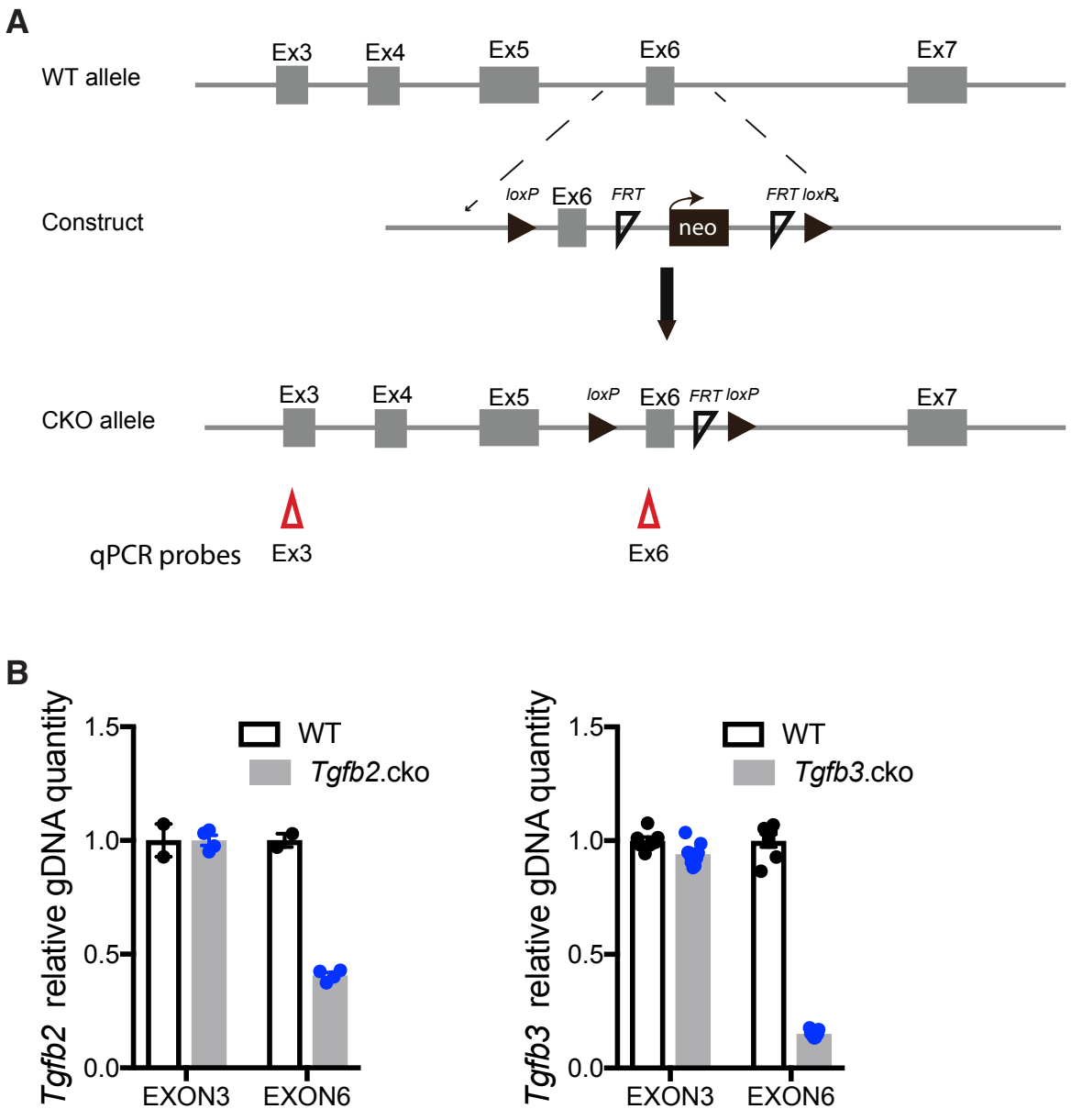

Fig. S5. Schematics of TGFβ2 and TGFβ3 conditional knockouts. (**A**) *Tgfb2* and *Tgfb3* conditional knockouts share a similar schematic. Two targeting constructs were targeting exon 6 in the *Tgfb2* or *Tgfb3* locus, respectively. Adeno-FLP was used to treat positive ES clones to remove the PGK neomycin selection marker at the ES cell stage. Two loxP sites were created to flank the exon 6 in the TGFβ2 or β3 loci in their respective cKO mice. Schematics are not drawn to scale. The positions of qPCR probes used in (B) are indicated with red triangles. (**B**) Lung genomic DNAs were isolated from

tamoxifen treated mice and evaluated by quantitative PCR (vs. *Tert*). Exon 3 is located outside of the floxed locus and was used as the experimental control. For TGFβ2, WT mice (n=2); cKO mice (n=4); for TGFβ3, WT mice (n=7); cKO mice (n=9).

A

K_D (nM)	Human β2	mouse β2
6F12	<0.001	<0.001
4A11	0.008	<0.002

B

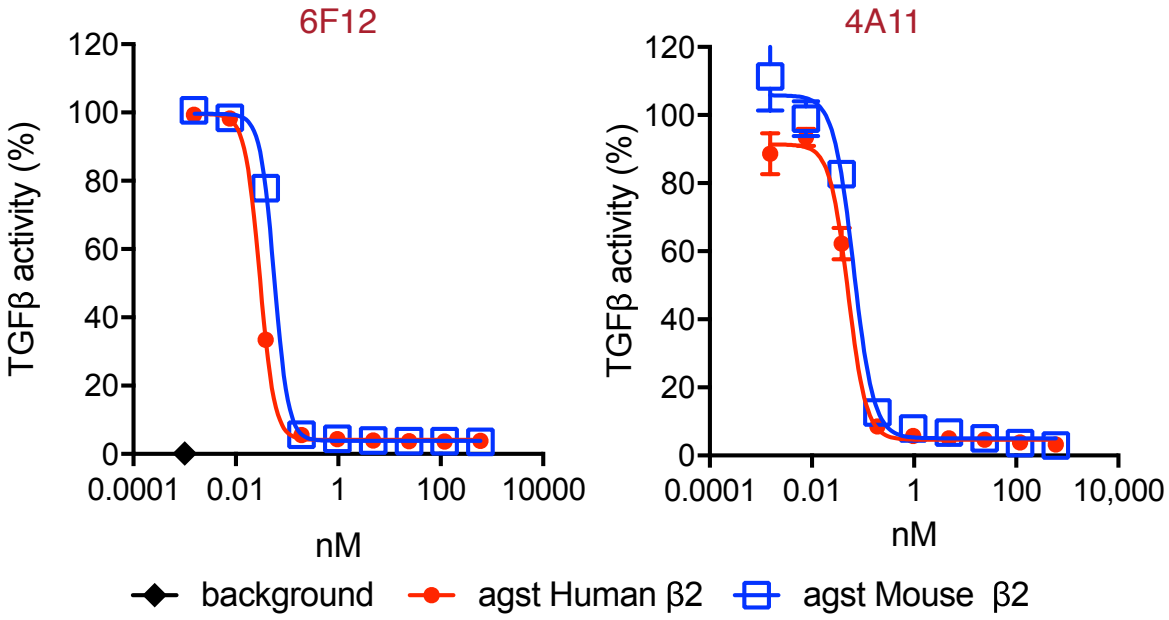

Fig. S6. 6F12 and 4A11 inhibit mouse and human TGFβ2 comparably. (**A**) The affinity (K_D) of human or mouse TGFβ2 peptide with the 6F12 or 4A11 antibody was determined by Biacore SPR. (**B**) Mature peptide (1ng/ml) of human or mouse TGFβ2 was incubated with a series of concentrations of 6F12 or 4A11 antibodies. TGFβ activities were measured with MLEC reporter cells. Curves are best fit to dose-response inhibition model. BKGD (background), no mature peptide added.

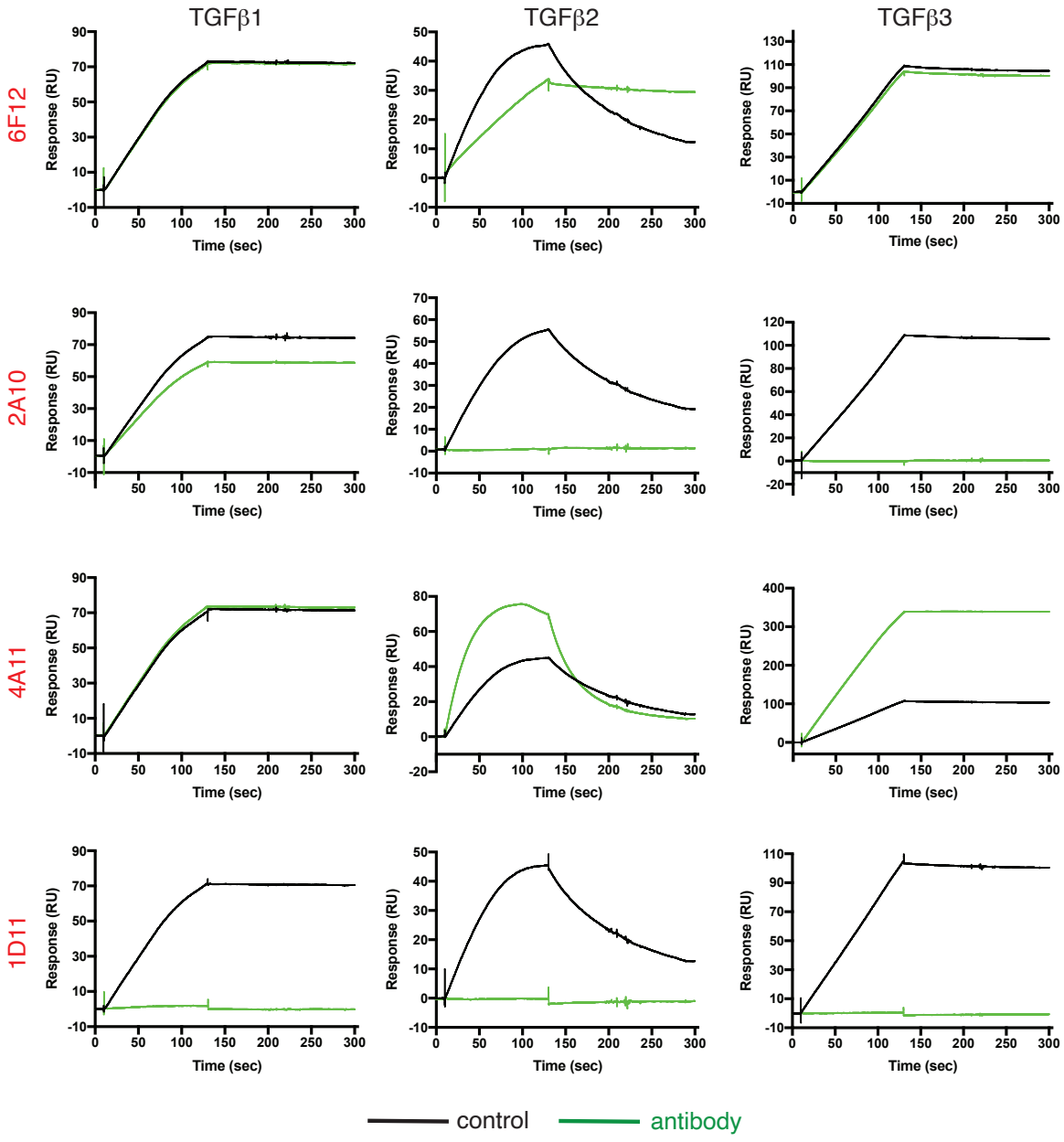

Fig. S7. Surface plasmon resonance sensorgrams for binding of the TGFβR2 to TGFβ ligands in the presence of anti-TGFβ antibodies. TGFβ isoforms were premixed with individual antibodies (1:10) before being applied to a surface with captured TGFβR2-Fc.

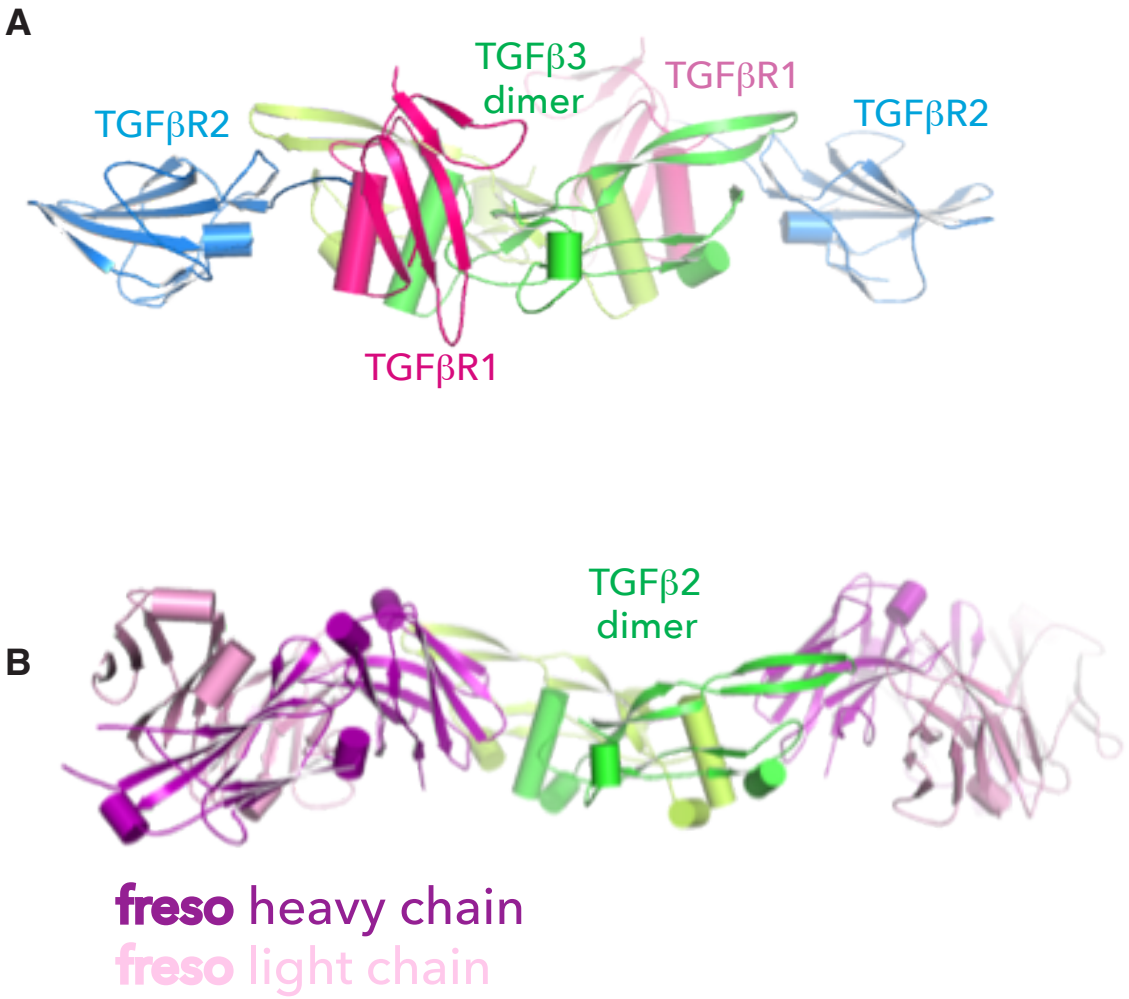

Fig. S8. 4A11 binds to a different epitope of TGFβ2 than the TGFβR complex. (**A**) Crystal structure of a TGFβ3 dimer (green) bound by the TGFβR receptor complex (R1, red; R2, blue) (PDB 2PJY) (*33*). (**B**) Crystal structure of a TGFβ2 dimer (green) bound by a pan anti-TGFβ antibody, fresolizumab (PDB 4KXZ) (*31*).

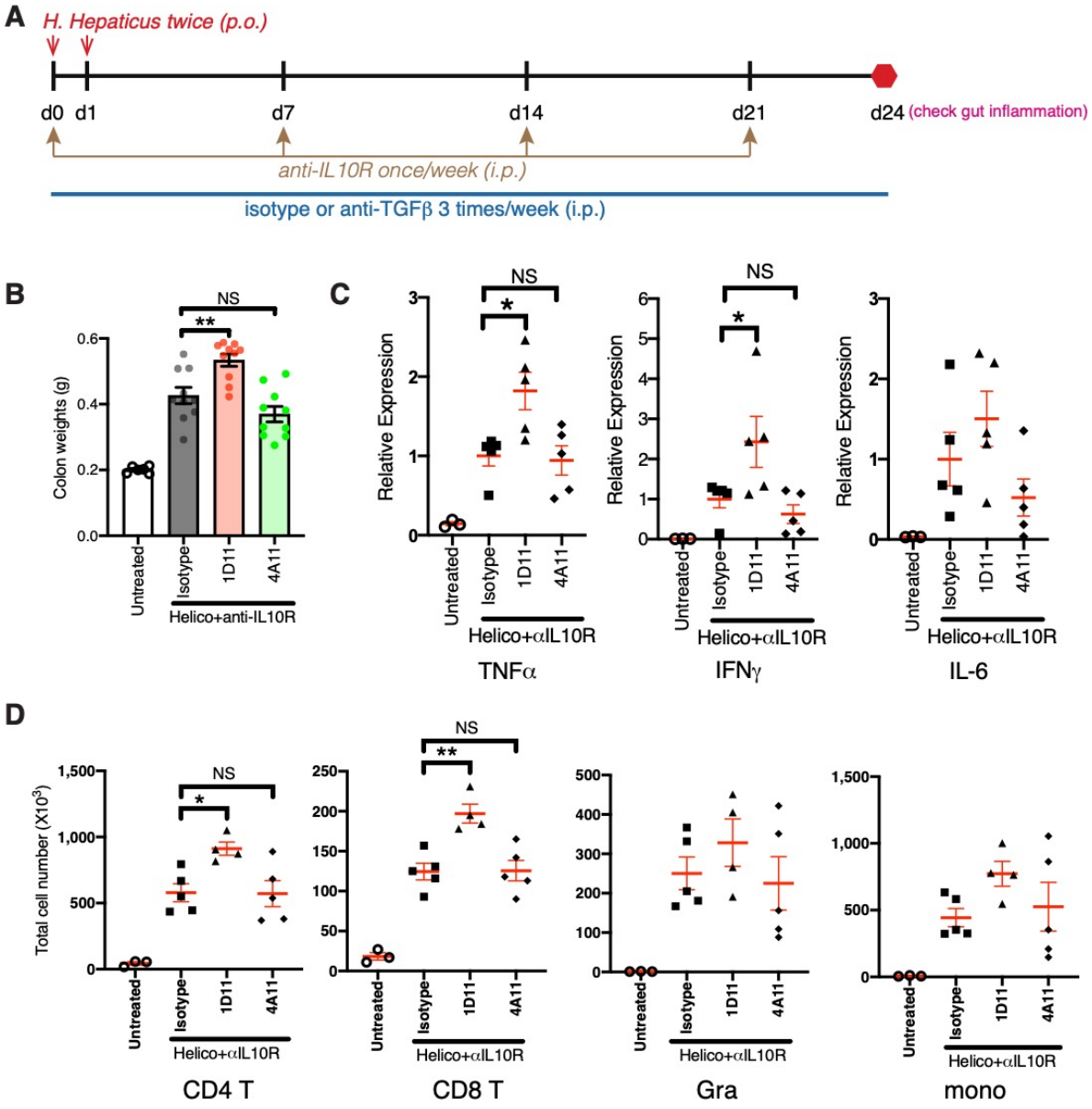

Fig. S9. TGFβ2 and TGFβ3 blockade does not lead to enhanced immune responses that are associated with pan anti-TGFβ antibody treatment. (A) Schematic for a colitis model to assess the enhanced inflammatory responses associated with anti-TGFβ antibodies. **(B)** Colon weights (grams) were measured at day 24. N=10 for all groups except the untreated group (n=6). **(C)** Colon RNA was analyzed for the expression of inflammatory genes. Three to five mice from each group were analyzed as indicated. **(D)** Immune cell numbers in lamina propria from the remaining mice in each group (3-

5/group) were determined by flow cytometry using their surface markers: T cells (CD3+; CD4+ or CD8+); Granulocytes ("Gra," CD11b+; Ly6G+); monocytes ("mono," CD11b+; Ly6C+). *P < 0.05, **P < 0.01, NS, P>0.05 by One-way ANOVA with Dunnett's test. Data represent means ± SEM. For clarity, stats bars are not shown in graphs lacking nominally significant differences between experimental groups.

Table S1: Characteristics of isoform-selective anti-TGFβ monoclonal antibodies.

		A			B			C			D
		Cell-based IC50 (nM)			SPR Affinity K_D (nM)			Blocking of TGFβR2 & TGFβ			Blocking of TGFβR3 & TGFβ2
Specificity	**Clone**	**TGFβ1**	**TGFβ2**	**TGFβ3**	**TGFβ1**	**TGFβ2**	**TGFβ3**	**TGFβ1**	**TGFβ2**	**TGFβ3**	
αTGFβ2	**6F12**	>600	0.04	>600	>15	<0.001	>15	NB	D	NB	B
αTGFβ3	**2A10**	>600	193	0.02	1.6	0.046	<0.002	NB	B	B	n.d.
αTGFβ2/3	**4A11**	>600	0.25	0.03	>15	0.008	0.005	NB	E	E	B
α-Pan-TGFβ	**1D11**	0.5	3.6	0.04	0.038	0.009	0.007	B	B	B	n.d.

(A) The potency (IC50) of each TGFβ selective antibody was assessed by inhibition of TGFβ-induced TGFβR-dependent signaling in reporter cell lines (HEKBlue) at 37°C. **(B)** The affinity (K_D) of each TGFβ selective antibody was determined by Biacore SPR under the format of detecting TGFβ binding against surface captured antibody at 25°C. **(C)** The blocking capability of each antibody was assessed by Biacore SPR. TGFβ were premixed with individual antibody (1:10) before applied to the surface captured TGFβR2-Fc. **(D)** The blocking capabilities of 6F12 and 4A11 were assessed by Biacore SPR. Recombinant TGFβR3 was premixed with TGFβ2 in a series of dilutions before applied to the surface captured antibodies. NB, not block; B, block; D, disturbed; E, enhanced; n.d., not done.

Table S2: Characteristics of the humanized 4A11 clone.

Version	Cell-based IC_{50} (nM)			SPR Affinity K_D (pM)		
	TGFβ1	TGFβ2	TGFβ3	TGFβ1	TGFβ2	TGFβ3
Rabbit 4A11	>200	0.48	0.020	>5000	1.6	<1.2
Humanized 4A11	>200	0.22	0.033	>5000	6.3	9.7

The rabbit 4A11 antibody was humanized using available human germlines in the international immunogenetics information system (Lefranc et al., 1999). The TGFβ inhibition potency and binding affinity of the humanized 4A11 antibody were comparable to the rabbit 4A11.

Lefranc, M.P., Giudicelli, V., Ginestoux, C., Bodmer, J., Muller, W., Bontrop, R., Lemaitre, M., Malik, A., Barbie, V., and Chaume, D. (1999). IMGT, the international ImMunoGeneTics database. Nucleic acids research *27*, 209-212.

Table S3: Data collection and refinement statistics for TGFβ2/4A11 structures.

	TGFb2/4A11
Data collection	APS 22ID
Space group	P1
Cell dimensions	
a, *b*, *c* (Å)	64.42, 85.11, 112.73
α, β, γ (°)	112.73, 99.15, 97.32
Resolution (Å)	82.97-1.91 (20.1-1.91)
R_{sym} or R_{merge}	0.073 (0.494)
I / σI	8.5 (2.5)
Completeness (%)	90.5 (88.7)
Redundancy	2.8 (2.9)
CC1/2	0.997 (0.877)
Refinement	
Resolution (Å)	82.97-1.91
No. reflections (total/test)	161613/8036
R_{work} / R_{free}	20.5/24.4%
No. atoms	
Protein	16444
Water	708
B-factors	
Protein	41.7
Water	42.4
R.m.s. deviations	
Bond lengths (Å)	0.10
Bond angles (°)	1.19

*Values in parentheses are for highest-resolution shell.

Table S4: Amino acids in the 4A11 epitope interacting with TGFβ2 dimers.

TGFβ2 chain A	Light Chain	Heavy Chain
V313		S28; S30; S31
Q314		S28; S30
D315		S28; L29; S30; S73
R320		S30
P321		Y53; G102; G103
L322		Y53; G103
Y323		G103; A104; P105
R328	Y30; N31	P105
D329	Y30	
F345		Y53; G54
A347		G54

TGFβ2 chain B	Light Chain	Heavy Chain
N368	G96; K100	S56; Y58
T369	S95; G96; S97; K100	Y58
I370	Y30; Y94; S95; G96; K100	
N371	Y30; Y94; S95; K100	Y50
P372	A30; A34; G93; Y94; S95; K100; Y101	Y50
E373	Y101	T33; Y50; Y53; H98; Q100; V101; G102; G103; G107; S108
A374	K100	S52; Y53; G54; S56; Y68
S375		Y53; G54; G55; S56;
A376		G55; S56
S377		S56

Table S5: Primary amino acid sequences at various positions among TGFβ1, β2, β3 that interact with the 4A11 epitope.

TGFβ2	TGFβ3	TGFβ1
D315	E	K
R320	R	R
Y323	Y	Y
R328	Q	K
D329	D	D
F345	F	F
Y352	Y	Y
N368	N	N
T369	T	Q
I370	L	H
N371	N	N
P372	P	P
E373	E	G
A374	A	A
S375	S	S
A376	A	A
S377	S	A

Table S6: Anti-TGFβ isoform-specific antibodies all exhibited favorable pharmacokinetics in C57BL/6 mice.

Antibodies	Specificity	Route	Dose (mg/kg)	C_{max} (μg/mL)	AUC_{last} (day•μg/mL)	CL (mL/day/kg)	$T_{1/2, \lambda z}$ (day)
6F12	TGFβ2	IV	1	23.3	104	4.89	10.2
		IV	10	273	1163	3.88	15.5
		IP	10	134	1197	3.58	17.5
2A10	TGFβ3	IV	10	305	1910	3.56	13.1
4A11	TGFβ2/3	IV	1	18.1	118	4.58	10.6
		IV	10	233	1486	4.16	9.2
		IP	10	133	1456	4.39	5.5

C_{max} = maximum observed concentration; AUC_{last} = area under the serum concentration versus time curve from time = 0 to time of the last measurable concentration; CL = clearance; $T_{1/2, \lambda z}$ = terminal half-life

Data file S1. raw data.